TÉCNICO LISBOA

The impact of aromatic admixture on *n*-alkane hydrocracking over Pt/HUSY

Bernardo Alves Canudo

Thesis to obtain the Master of Science Degree in

Chemical Engineering

Supervisors: Professor Doctor Pedro Simão Freitas Mendes

Doctor Nebojsa Korica

Examination Committee

Chairperson: Professor Doctor Isabel Maria Delgado Jana Marrucho Ferreira

Supervisor: Professor Doctor Pedro Simão Freitas Mendes

Members of the Committee: Professor Doctor Maria Filipa Gomes Ribeiro

November 2022

Acknowledgments

I would like to thank to my supervisor Professor Doctor Pedro Mendes, for the opportunity to work on my thesis outside of Portugal, away from the comfort of what I know, allowing me to challenge myself and grow, both on a professional and personal level. For all the support, insights and availability throughout the entire process. I would like to express my gratitude to my coach Nebojsa Korica, from Ghent University. For all the patience, support and time spent on teaching and supporting me. For all the suggestions and availability to help me with any doubts and technical challenges that appeared during my stay abroad.

A special thank you to Rodrigo, Natascha and Nacho who were kind enough to let strangers into their house during our troubled first weeks in Ghent. This is something I will never forget. To the friends who accompanied me through the ups and downs of this journey, Diogo, Filipe, Jéssica we did it. To the people who I met in Ghent, especially the residents of the Holiday Inn who helped make this experience even more memorable.

To my friends back home, who watched me grow and were there every step of the way, a special thank you.

This marks the end of my amazing journey at Técnico, it is something that cannot be described by words. To my godmother Tânia, who helped me through it all, and made me see that it could be done. For all the hours spent studying together, for all the Zoom calls, for every conversation with friends, for all the partying, for all the *jolas*, for the *primos* and *primas*, for all the moments we shared together, for the family I earned at this university, for the friends who helped make these last five years even more special. I am truly grateful.

Gostaria de agradecer a toda a minha família, que me apoiou durante esta jornada. Às minhas duas avós Emília e Maria Luísa que são um exemplo de força, coragem e determinação. À minha irmã Bianca, que desde sempre me inspirou a encarar a vida com coragem e firmeza, mas sempre com um enorme sorriso nos lábios. Agradeço também aos meus avôs, António e José, que sempre me acompanharam e tenho a certeza que estariam orgulhosos do quão longe o neto chegou. Esta conquista também é vossa.

E como o melhor fica para o fim, quero deixar um enorme obrigado aos meus pais, Luís e Miriana que não só me suportaram durante estes cinco anos de universidade, mas que desde cedo me incutiram valores de curiosidade, trabalho e bondade que me permitiram chegar até aqui. Obrigado por todo o amor, carinho, confiança e por me encorajarem sempre a ser melhor. A vocês devo tudo, nunca conseguirei repagar-vos nem metade daquilo que me deram. Obrigado.

"Nem todos podem ser grandes artistas, mas um grande artista pode surgir em qualquer lado"

Abstract

Historically, hydrocracking was used as an answer to the increases in demand of middle distillate petrochemical products paired with higher crude oil prices, since hydrocracking allowed for the valorization of heavy oils into high-value middle distillates. Nowadays, hydrocracking of pure vegetable oils or in mixture with heavy oils is seen as a great opportunity for the production of biofuels, as a way towards better energy sustainability worldwide.

The present work allowed for an insightful understanding of the effects of the addition of aromatic molecules on the hydrocracking of *n*-alkane, by following alkane conversion, isomer selectivity, and catalyst deactivation at different conditions, over a proven well-balanced Pt/HUSY catalyst. *n*-octane and toluene were used as model components. By studying the conversion and the product distribution, it was possible to understand the mutual admixture impact of reactants on the reaction which included also identifying transitions in hydrocracking regime.

When sufficiently high hydrogen-to-hydrocarbon ratio (80 - 200) was used, the catalyst stability, conversion and isomer selectivity of *n*-octane remain unchanged, meaning that the addition of toluene did not induce a shift from ideal to non-ideal hydrocracking. Toluene was completely converted to hydrogenation products.

Lowering hydrogen-to-hydrocarbon ratio (6.5) resulted in catalyst deactivation at all process conditions. The deactivation was stronger at lower applied pressure which could be related to more likely bimolecular reactions of aromatics on acid sites. Toluene conversion was not complete and products of reactions on acid sites without prior hydrogenation, were detected. These products (benzene and xylenes) are considered as responsible for catalyst deactivation as they lead to coke formation. At higher temperatures, non-ideal hydrocracking was observed due to the impact of toluene reactions on both active sites of the catalyst, coupled with the effects of changing process conditions.

Optimization of hydrogen-to-hydrocarbon ratio appears to be the way to control the effects of aromatic molecules on alkane hydrocracking, since it promotes hydrogenation of aromatic molecules thus avoiding bimolecular reactions on acid sites which lead to catalyst deactivation. In an industrial setting, this ratio could be increased by using higher hydrogen flowrate. Despite of this, further investigation is needed to better understand the conditions upon where the addition of aromatic molecules is enough to impact the metal to acid site ratio of the catalyst and thus induce a shift in hydrocracking regime.

Keywords: Hydrocracking, metal/acid site ratio, aromatic impact, catalyst activity.

Resumo

Historicamente, *hydrocracking* é usado como uma resposta à crescente procura de destilados médios, juntamente com o aumento de preço do petróleo bruto, visto que permite a valorização de óleos pesados. No entanto, recentemente o processo de *hydrocracking* tem vindo a ser explorado como uma excelente oportunidade para a produção de biocombustíveis, usando óleo de cozinha puro ou em mistura com óleos pesados, de modo a caminhar para uma economia de combustíveis mais sustentável.

Esta investigação permitiu a compreensão dos efeitos da adição de aromáticos ao processo de *hydrocracking* de um *n*-alcano. Isto foi atingido através do estudo da conversão e seletividade para isómeros do alcano e da desativação do catalisador Pt/HUSY sobre diferentes condições operatórias. *n*-octano e tolueno foram usados como moléculas modelo. Através da análise da distribuição de produtos e conversão, foi possível compreender os impactos mútuos dos dois reagentes na reação, bem como identificar transições no regime de *hydrocaking.*

Quando a razão entre hidrogénio-hidrocarboneto usada era relativamente elevada (80-200), observou-se que a estabilidade do catalisador, conversão e seletividade para isómeros de *n*-octano permaneceu constante. Isto implica que a introdução de tolueno não resultou numa mudança de regime de *hydrocracking*. Nestas condições, tolueno foi completamente convertido em produtos de hidrogenação.

A diminuição da razão entre hidrogénio e hidrocarboneto para 6.5 resultou na desativação do catalisador, independentemente das condições operatórias usadas. Esta desativação foi mais pronunciada a pressões mais baixas, o que pode ser relacionado com a maior probabilidade de ocorrência de reações bimoleculares entre aromáticos nos sítios ativos ácidos do catalisador. A conversão de tolueno não foi completa, e foi possível detetar produtos provenientes da reação de aromáticos nos sítios ativos ácidos do catalisador, sem hidrogenação prévia (benzeno, xilenos). Estes produtos são responsáveis pela desativação do catalisador, dado que resultam na formação de coque. O aumento da temperatura resulta na transição para *hydrocracking* não ideal, não só devido ao impacto do tolueno nos sítios ativos do catalisador, mas também devido aos efeitos da alteração das condições operatórias do processo.

A otimização da razão hidrogénio-hidrocarboneto permite controlar os efeitos da introdução de aromáticos no processo de *hydrocracking* de um dado *n*-alcano. A nível industrial, esta razão pode ser aumentada usando um maior caudal de hidrogénio, de modo a prevenir a desativação do catalisador através da redução do número de reações entre moléculas aromáticas nos sítios ativos do catalisador. Apesar disto, outras investigações serão necessárias para melhor compreender as condições sobre as quais a introdução de aromáticos é suficiente para perturbar a razão entre sítios metálicos e ácidos do catalisador, levando à mudança de regime de *hydrocracking*.

Palavras-chave: *Hydrocracking*, razão sítios ativos metálicos/ácidos, impacto aromático, atividade catalítica.

Table of Contents

List of Figures

List of Tables

List of Symbols

FCC: Fluid Catalytic Cracking

Mbd: Million barrels per day

PCP: Protonated cyclic propanes

n_{Pt}/n_{H+}: metal-to-acid site ratio

H_2/HC: hydrogen-to-hydrocarbon ratio

I/C: Isomerization/cracking ratio

HTK: high throughout kinetic setup

GC: Gas chromatograph

FID: Fire ionization detector

BET: Brunauer–Emmett–Teller

ICP-OES: Inductively Coupled Plasma Spectroscopy: Optical Emission Spectrometry

TEM: Transmission Electron Microscopy

NH_3-*TPD*: ammonia temperature-programmed desorption

H_2-*TPR*: Hydrogen temperature-programmed reduction

TOS: Time on stream

1. Introduction

1.1 The hydrocracking industry and market

During the last century, mankind has witnessed a huge increase in the demand for products from the oil refining industry, mainly due to the appearance of several scientific discoveries, the worldwide economical and industrial growth, and the increase in cost of living. These factors coupled with the increasing trend of crude prices [1], the forecasted decrease in fossil fuels demand and the increase in bio-fuels interest [2]–[4] led to the study and introduction of processes capable of converting heavy oil fractions into lighter high value products. These are more difficult to process than their lighter counterparts and have relatively low economic values prices [1] which means that finding a way to upgrade them results not only in better distillate yields of products with increasing demand such as kerosene, jet fuel, diesel or naphtha [5], but also in a decrease of the amount of residue that could goes untreated, which represent additional expenses for the refinery.

Stricter environmental regulations have also been created to limit the content of certain noxious components (sulfur and aromatics) in fuel, reducing the amount of harmful gas emissions while enhancing motor performance. Despite lower refractory aromatics concentrations, these components are always present in the hydrocracking feed, meaning that is important to understand their impact on the hydrocracking reaction. As an example, Table 1 shows the reduction in sulfur and aromatic content in gasoline and diesel over the years. [6]

Table 1: Evolution of oil products specifications. [6]

Refinery product	Product specification			
	Before 2000	2000	2005	2009
Gasoline				
Sulfur (ppm)	500 max.	150 max.	50 max.	10 max.
Aromatics (% v/v)	none	42	35	35
Diesel				
Sulfur (ppm)	500 max.	150 max.	50 max.	10 max.
Polycyclic aromatics (% m/m)	none	11	11	8

In recent years, hydrocracking has been studied as a good solution to produce biofuels, reducing global dependence on crude oil and reduce pollution [7]–[9]. Producing biofuels by hydrocracking uses infrastructure already present in oil refineries [10], reducing the amount of initial investment needed. Hydrotreatment of vegetables oils results in fuel with better properties than biodiesel produced through transesterification [7] and the use of mixtures comprised of vegetables oils and vacuum gas oils could also be used as feedstock, as shown by some investigations [11]. Current biofuel production processes require big investments to ensure high efficiency and produce great amounts of glycerin, which presents an environmental problem since it contains salt, free fatty acids and methanol that contaminate the soil where this byproduct is

thrown away [12]. The price and availability of fresh vegetable oils are also a concern for these technologies. [7][8] With this in mind, used cooking oil has shown to achieve similar yields of biodiesel as fresh cooking oil, proving that this feedstock could be the key for the production of biofuels through hydrocracking. [8] Hydrocracking process could prove to be central in transition towards a more sustainable fuel economy.

Cracking processes are used to break long chain hydrocarbon molecules, where at least one of the carbon-carbon bonds is ruptured, generating two smaller hydrocarbons. This reaction can occur by means of four distinct mechanisms, with or without catalyst and dependent on applied process conditions:

- Hydrocracking: Uses a bifunctional catalyst, which has metal and acid sites, where different chemical reactions take place. The metal is responsible for the dehydrogenation of saturated hydrocarbons into alkenes. After diffusion into the acid sites, these species are protonated to carbenium ions which undergo different isomerization/cracking reactions. The formed carbenium ions are consecutively hydrogenated on the metal sites to the reaction products [13][14]. The process takes place in a hydrogen-rich atmosphere at temperatures between 260 °C and 425 °C [15], and pressures of 35 bar to 200 bar [15], depending on the desired product distribution and on the specific role of the hydrocracking unit in the refinery complex.

- Hydrogenolysis: This process is applied in petroleum refineries to remove heteroatoms such as sulfur, nitrogen or oxygen from hydrocarbon feeds, while also being used for hydrocarbon cracking [16] and is catalyzed by metallic monofunctional catalysts. The cleavage of the chemical bond is followed by the simultaneous addition of a hydrogen atom to the obtained molecules [17]. It takes place under atmospheric pressure with temperatures between 150°C and 200°C.[18][14]

- Catalytic cracking: This is the standard term for cracking utilizing monofunctional acid catalysts and it can be subdivided in two, according to the mechanism that is followed: monomolecular via carbonium ions (also known as Haag-Dessau cracking) or bimolecular cracking with carbenium ions [14]. Among different catalytic cracking processes, Fluid Catalytic Cracking (FCC) is the most popular one and requires temperatures in the range of 400°C to 550°C [19] and 2 bar of pressure. [20]

- Thermal cracking: The cracking reaction involves radicals as intermediates which is achieved by working with harsher conditions, temperatures of 500°C to 600°C and high hydrogen pressures [14]. This process does not require any catalyst.

The first process for breaking down large hydrocarbon molecules appeared in 1913, suffering several different improvements over the years and in 1936 the first catalytic cracking processes came into use. Hydrocracking only started gaining industrial relevance by the 1950s due to the increase in demand of automobile and jet fuel [21] and increase in crude oil prices paired with the increased research on higher efficiency processes for the processing of crude oil. The first modern hydrocracking industrial installation was owned by the Standard Oil Company of California.

Castaneda and coworkers [1] showed that thermal cracking processes such as visbreaking and coking still represented more than half of the capacity to manage and reuse industrial residue, mainly due to its low investment costs. Table 2 shows the relative worldwide capacity of different cracking technologies.

Table 2: Worldwide capacity distribution of cracking technologies. [1]

Technology		% Capacity Worldwide
Thermal Cracking	Visbreaking	26,76
	Coking	31,69
Hydroconversion	Hydrocraking	14,52
	Hydrotreating	3,20
Catalytic Cracking (FCC)		23,83

A decade later, the worldwide capacity distribution remains relatively unchanged. In 2020, the global refinery hydrocracking unit's capacity was 11 683 mbd [22], which still falls short in comparison with the FCC global capacity over the same period (14 259 mbd [23]). However, the capacity and number of hydrocracking units has been increasing at a considerable rate due to the advantages this process possesses over other cracking methods. Although hydrotreating operations carry higher operational and capital costs, the increase in fuel prices and stricter environmental legislations favor the use of different technologies such as hydrocracking to reach higher yields of desired products while also reducing the amount of residual fuel oil produced. Hydrocracking presents other benefits, namely being less prone to coking, being able to obtain better isomer yields and having a broad range of products that can be manipulated by altering the process conditions or the catalyst used. [15][24]

2. State of the art

2.1 Catalyst

Hydrocracking of *n*-alkanes requires a catalyst with two distinct types of active sites: metal and acid sites. This is known as bifunctional catalyst. The function of the metal site is to dehydrogenate the feed alkanes into alkenes and the acid sites are used for elementary isomerization and cracking reactions of protonated intermediate alkenes. The balance between metal and acid site strength is responsible for product distribution and for the observed hydrocracking regime, which will be further explained in later sections.

2.1.1 Metal function

The objective of the metal is to promote the dehydrogenation of alkanes before they undergo isomerization and cracking reactions on the acid active sites of the catalyst. The most used metals are nickel (Ni), platinum (Pt), palladium (Pd), cobalt (Co), tungsten (W) and molybdenum (Mo) [24]. In hydrocracking, one of the most important properties of the metal function is its hydrogenation strength, which varies depending on the metal element, concentration and dispersion. The metal is deposited on the acidic support via incipient wetness impregnation or ion exchange.

Several investigations on monometallic catalyst show that noble metals such as Pt and Pd have higher activity and stability when compared to other metals but are more prone to being poisoned by sulphur compounds [2], which leads to the application of expensive metal recovery processes. Between noble metals, Pt shows higher hydrogenation capacity than Pd [25], regardless of what alkane was used. Alternatively, catalysts with Co/Ni/Mo/W as metal function are more prone to coking and have lower hydrogenation capacity than noble metals but have relatively low manufacturing costs, which makes them the dominant catalyst type in many industrial applications. [26]–[28]

For this investigation, platinum was used as the metal function of the bifunctional catalyst given its high hydrogenation capacity and stability.

2.1.2 Acid function

The acid function is responsible for the cracking and isomerization reactions. Zeolites are the most studied acidic supports for bifunctional catalyst given that they combine high acidity, activity and stability and good regeneration capabilities. Aluminophosphates based supports can be used as an alternative to zeolites despite having weaker acid sites which could make them suitable to use in selective alkane isomerization [24]. In cases where diffusion limitations are observed, alumina or silica-alumina based materials can be used as replacement for certain zeolites, allowing for improved accessibility to the active sites of the catalyst.

Zeolites are aluminosilicates with three-dimensional crystal structures composed of tetrahedral framework where each oxygen atom is shared by two other tetrahedra (with molecules of either SiO_4 or AlO_4). To compensate for the negative charges introduced by the presence of alumina atoms in the silicate framework, the micropores of the zeolite include counterions and water molecules. The microscopic structure of faujasite/Y is shown in Figure 1, as an example. This three-dimensional structure creates pores, channels and cages in regular arrangement with molecular dimensions, which makes them highly suitable for catalysis since the spaces inside the framework can be manipulated to control access to active sites.

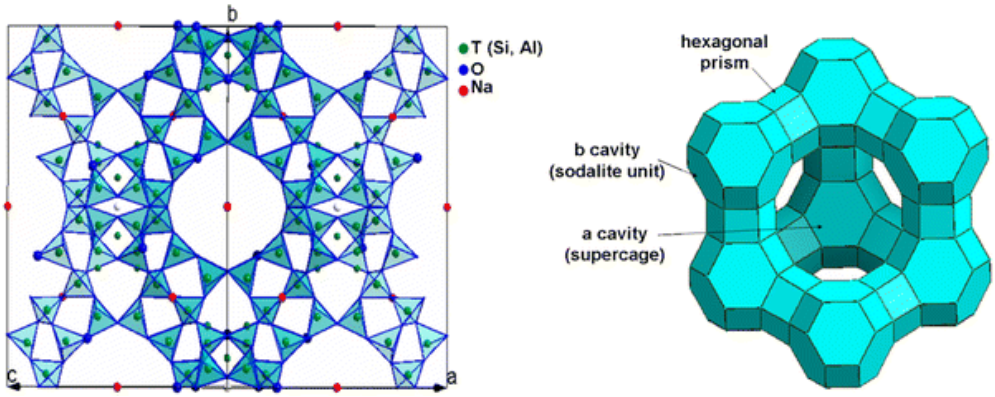

Figure 1: Microscopic structure of faujasite framework, assembled from SiO4 tetrahedra. [29]

Zeolites contain both Brønsted and Lewis acid sites and their concentration, strength and location impact the overall activity, selectivity and stability of the catalyst. [30] The strength of Brønsted acid sites depends on the electronegativity of the surrounding cations (Si^{4+} or Al^{3+}), as seen in Figure 2. The strongest acid sites are the ones where the second coordination sphere contains six Si^{4+} ions, decreasing in strength with the increase of Al^{3+} atoms [31]. Due to this relationship, it has been found that zeolites with low Al^{3+} concentration have a low density of high strength acid sites while zeolites with higher Al^{3+} content have higher density of acid sites, but these acid sites have lower strength. [31]

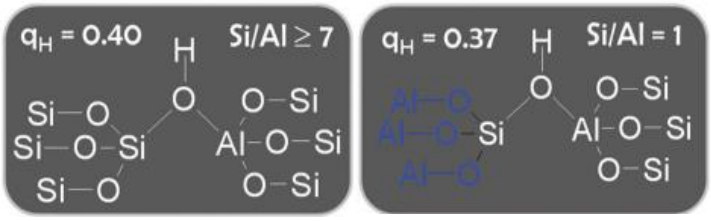

Figure 2: Influence of the surrounding atoms on the strength of Brønsted acid site. [31]

Due to a slighly higher ionic radius of Al^{3+} (in comparison to Si^{4+}), the presence of Al atoms induces instability to the zeolite framework which results in the migration of Al^{3+} forming octahedrall Al species known as extra framework aluminium (EFAL) [31], which is responsible for the the Lewis acidity of the zeolite.

The overall acidity of a zeolite is also influenced by its structure. Zeolite properties such as pore size and orientation are dependent on its structure which is determined not only by the secondary building unit but also how those units are connected to each other.

Nowadays, more than 200 zeolites and zeotype are recognized with only a small percentage of them being applied in commercial processes. Out of this number, Vogt et al. [32] distinguished five zeolites (known as “Big Five”) as the ones that are produced in significant amounts for catalytic applications: faujasite, ZSM-5, beta polymorph A, mordenite and ferrierite.

Faujasite X and Y have a three-dimensional structure that consists in sodalite cages (or β cages) connected through hexagonal prisms. [18][27] When the Si/Al ratio of the faujasite is close to one, they are usually designated as X-zeolite, while in cases where the Si/Al is higher than two they are denoted by Y-zeolite [33]. The Si/Al ratio of Y zeolite can be enhanced by dealumination resulting in ultra-stable Y zeolite (USY) which is hydrothermally more stable, and more selective towards middle distillates. [33]

ZSM-5 consists in two types of intersecting small 10-membered pore channels, which are smaller than the pores found in beta/faujasite, leading to stronger diffusion limitations, promoting consecutive reactions of isomerization and cracking on acid sites. [24][33]

The beta zeolite is composed by two different 12-membered rings with different diameters. In both channels the pore size is lower than the faujasite pores however, the beta zeolite is still considered as large-pore zeolite and was found to result in a similar hydrocracking product distribution despite different selectivity towards certain products due to its narrower pore structure and reduced super-cages. [33]

The mordenite framework can be divided into pores with two different diameters, the larger ones and the smaller ones, which can be referred as “side pockets”. The two channels are connected by small elliptical openings which makes interconnectivity relatively difficult, meaning that the channel system is essentially works as one-dimensional [29] and the access to all acid active sites is limited. This characteristic of the mordenite zeolite leads to diffusion limitations and higher cracking selectivity, which makes the mordenite zeolite more prone to the formation of coke and consequent deactivation. [24][33][34]

The framework of ferrierite is a two-dimensional channel structure consisting of larger 12-membered rings and smaller 8-membered oval-shaped side channels. Both types of channels 7 are relatively small meaning that ferrierite is considered as a medium pore-size catalyst with strong diffusion limitations. [30][35]–[37]

The most widely used catalyst for hydrocracking is the Y-type [38], as it displays high activity and high selectivity towards alkane isomerization products, when compared with mordenite or HBEA catalysts [39], while presenting higher accessibility to active sites without spatial limitations related to molecule size. ZSM-5 is also commonly used in hydrocracking, as it shows higher

activity than beta and mordenite catalysts [40][41], however presents lower activity and selectivity towards isomerization than Y-type catalysts. [39][42]

One of the greatest advantage of zeolites when compared to other acidic supports is their higher acid strength which means that zeolites require lower temperatures to be used as hydrocracking catalysts while also being less prone to coke formation (and thus, deactivation) and more resistant to poisoning by sulphur and nitrogen compounds. Due to their microporous structure, mass transfer limitations are common inside the zeolite channels so zeolites with larger pores and three-dimensional structures (such as faujasite) provide less diffusion limitations, reducing the possibility of consecutive elementary reactions on acid sites. Zeolites are also generally preferred over other acidic supports for hydrocracking given their adjustable acid-basic properties, through different preparation techniques or post-synthesis treatments. [43]

2.1.3 Catalyst Stability

Catalytic activity and selectivity decrease with use due to several aging processes. This means that every catalyst has the need to either be replaced or activated after some time in use. Because of this, catalyst stability is an important issue for the chemical industry since catalyst degradation is unavoidable, which means that reducing its effects to a minimum while maintaining catalyst activity/selectivity at target levels results in larger profitable operation times. A common industrial practice to combat this is the increase in reactor temperature to maintain conversion during a run [44]. The deactivation rate of a given catalyst depends not only on its characteristics, but also on operating conditions and feed composition. [24]

Coke is a carbon rich solid material that is formed during the cracking of *n*-alkanes, cycloalkanes and aromatic molecules. It deposits on the catalyst surface, reducing access to active sites and thus reducing catalytic activity/selectivity. When microporous supports are used, coke deposits on the external surface of the catalyst, leading to blockage of the pores while in mesoporous supports the heavier molecules are diffused inside the pore and cover the acid sites. According to Gary and coworkers, with typical industrial hydrocracking feedstocks, the catalyst can be used during 2 to 4 years before the activity losses is large enough to warrant the regeneration of the catalyst [44]. This regeneration is done by burning off the coke deposits on the catalysts, and a single catalyst can undergo several times the regeneration process before having the need to be replaced. The catalytic activity after a regeneration cycle is similar to the level of the fresh catalyst [44], as shown in the investigation of Myers et al. [45], which followed the hydrocracking of cyclohexane and *n*-hexadecane over a Pt/SiO_2 catalyst. Hydrocracking is less susceptible to coke formation than other cracking processes due to the metal function of its bifunctional catalyst and the hydrogen atmosphere, which allow for the hydrogenation of coke precursors into stable products. [24]

Water is also a recurring presence in the reactor, either due to the conversion of oxygenates or by being dissolved in the feed. Yan and coworkers [46] studied the effects of water and *i*-pentanol on the hydrocracking of *n*-hexadecane over Pt/HY catalyst. It was observed that

the introduction of water resulted in the loss of catalytic activity given that water molecules were in competition with *n*-hexadecane for the catalyst active sites. The deactivating effect of *i*-pentanol can also be explained by this since this species is dehydrated into pentene and water. However, this effect was reversed, and the original catalyst activity was reached by drying with hydrogen [46]. In the work of Myers et al. [45] water was also the responsible for the observed loss in catalytic activity since it steams down the catalyst surface area.

Compounds which contain sulfur and nitrogen are common poisons in the hydrocracking since they tend to adsorb on both active sites (acid and metal) of the catalyst. Work by Galperin [47] showed the influence of these organic compounds (hydrogen sulfide – H_2S; tertiary butylamine – TBA) on the hydrocracking of *n*-decane over Pt catalysts (SAPO-11, SAPO-34, MAPSO-31). The introduction of H_2S and TBA as standalone components resulted in a decrease in catalyst activity, due to the poisoning of acid (nitrogen) and metal (sulfur) sites. A reduction in isomer selectivity was also observed, likely due to the change in balance between the active sites of the catalyst. However, when fed together, isomer selectivity remained similar to the one observed with unpoisoned Pt catalysts. The addition of the nitrogen compound neutralized all the strong acid sites, which was compensated by an increase in temperature (around 100 °C), which resulted in the increased activity of weak/intermediate active sites. The higher temperature also impacted the Pt-PtS equilibrium, shifting it towards the Pt side and improved metal activity, which means that a balance between the weak/intermediate active sites and the strong metal function is sufficient to ensure high isomer selectivity. [47]

2.2 Hydrocracking mechanism over bifunctional catalyst

Hydrocracking requires both a metal and an acid site and hydrogen as co-reactant to successfully transform *n*-alkanes into lighter products. This reaction mechanism was first introduced in the 60s by Weisz and confirmed by Coonradt and Garwood [24][48] and can be observed in Figure 3 [24][49]. Hydrocracking occurs over bifunctional catalyst with metal and acid sites with each type of active sites having different functions on the mechanism that will be further analyzed in this chapter.

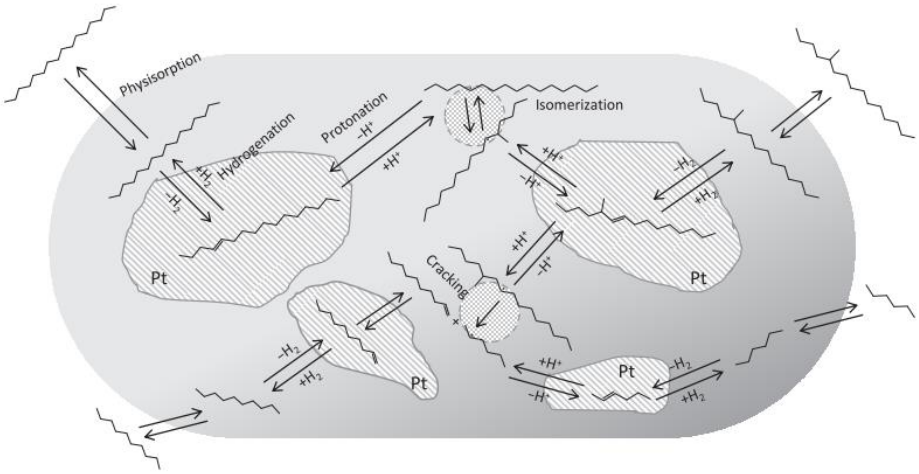

Figure 3: Bifunctional reaction scheme for the hydrocracking of n-hexadecane over Pt-loaded catalyst. [24]

2.2.1 Alkanes

The first step of the reaction scheme is the physical adsorption of the alkane in the micropores of the catalyst support by physical Van der Waals non-specific molecular interactions. The physisorption of hydrocarbons can be described using a simple Langmuir equation. The strength of these interactions between adsorbent (zeolite) and adsorbate (hydrocarbon) depends on different factors such as the topology of the zeolite and the nature of the adsorbed species as well as the conditions of temperature and pressure. [24]

In investigation done by Flinn and coworkers [50], it was found a considerable difference in conversion between *n*-hexadecane (95%) and *n*-octane (53%) using similar operating conditions over the same catalyst (Ni/SiO_2-Al_2O_3), which could not be explained solely by the increase in number of acid-catalyzed elementary reactions that results from higher carbon numbers. The answer was found with the work by Denayer et al. [51], where it was discovered that the values of physisorption enthalpy and entropy increase linearly with the increase in carbon number. It was also found that the enthalpy effect dominates over the entropy loss. [24][51]

Following the physical adsorption step, the first chemical reaction that occurs in alkane hydrocracking is the dehydrogenation of the hydrocarbon on metal site. According to literature,

this reaction follows the Horiuti-Polanyi mechanism [52][53], which is shown in Figure 4 [54]. This mechanism assumes all the catalyst surface sites are equal and consists of three steps that occur consecutively: adsorption of the alkane, dehydrogenation by cleavage of C-H bond and subsequent desorption of the alkene and the hydrogen molecule.

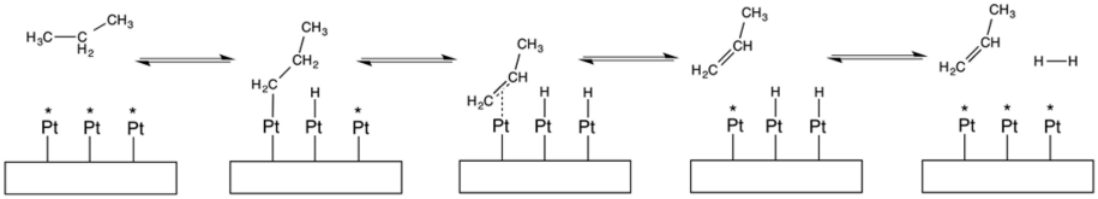

Figure 4: Horiuti-Planyi mechanism of the dehydrogentation of propane on platinum metal site. [54]

The presence of an olefinic intermediate in hydrocracking was proved by Weisz [55], that found that the product distribution obtained from *n*-dodecane hydrocracking over Pt/SiO_2-Al_2O_3 and 1-dodecene over Al_2O_3 were comparable. This was later confirmed by Coonradt and Garwood [48] in a similar experience, this time with the hydrocracking of *n*-hexadecane over Pt/SiO_2-Al_2O_3 and cracking of 1-hexadecene over an acid catalyst devoid of hydrogenation component (SiO_2-Al_2O_3) where the product distribution obtained from the two reactions was also similar. [24]

Following the dehydrogenation in metal site, the recently formed alkene is diffused to the acid side of the catalyst where it is protonated giving origin to an alkyl carbenium ion which will be the starting point for the elementary reactions of isomerization and cracking. Although some claim that the intermediate reactive species are surface alkoxyl, experimental results such as the ones obtained by Denayer and coworkers [56], tend to favor carbenium ions. [24]

Thybaut and coworkers [57] have shown that the protonation enthalpy is dependent on carbon number, decreasing from C_5 to C_8, however for molecules with more than eight carbon atoms this effect levels out and can be considered negligible. Protonation enthalpy for molecules with more than 8 carbon atoms depends solely on the type of carbenium ion that is formed upon protonation. The protonation reaction is shown in Figure 5.

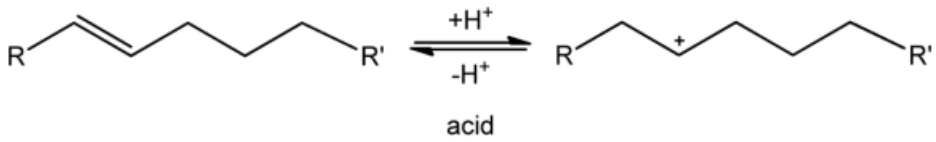

Figure 5: Reaction scheme of hydrocarbon protonation. [26]

Due to the unstable nature of primary cations [58], alkene protonation exclusively results in the formation of secondary and tertiary ions and these species can undergo reactions of two separate reaction families: isomerization or cracking.

Isomerization or skeletal rearrangements imply a change in the molecule structure without altering the number of carbon atoms and its usual to differentiate between type A or type B

rearrangements. Type A isomerization occurs through alkyl and hydride shifts reactions meaning that there is a change in the position of a side chain without altering the degree of branching. Alternatively type B rearrangements will result in the increase or decrease of branching level within the molecule and proceed via protonated cyclopentanes (PCP) intermediates. Although the mechanism of type B rearrangements has been a point of disagreement, evidence that supports PCP branching has emerged with the work of Martens and Jacobs in the study of *n*-decane transformation over Pt/USY and Pt/CaY catalysts [58] , but also the investigation conducted by Weitkamp [59] regarding isomer selectivity of long chain *n*-alkanes over Pt/CaY catalyst and Brouwer and Oelderik [60] who analyzed the isomerization *n*-butane in the super acid HF-SbF5. Both type A and type B reaction mechanisms are exemplified in Figure 6.

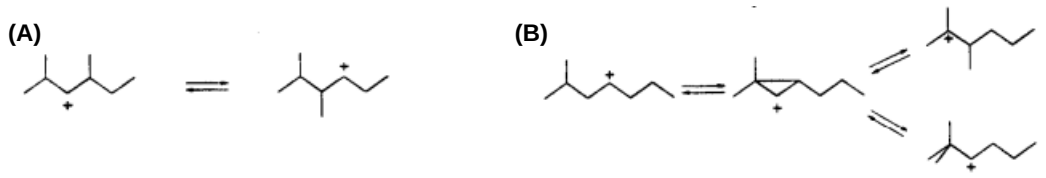

Figure 6: Reaction scheme for (A) type A isomerization (methyl shift) and (B) type B isomerization (PCP branching). [61]

The elementary cracking reactions occur by breaking the carbon bond in the beta position relative to the positive charge, hence the name β-scission, resulting in an alkane and a smaller carbenium ion. Depending on the nature of reactant molecules and obtained products, these cracking reactions are classified into five groups. [14][24]

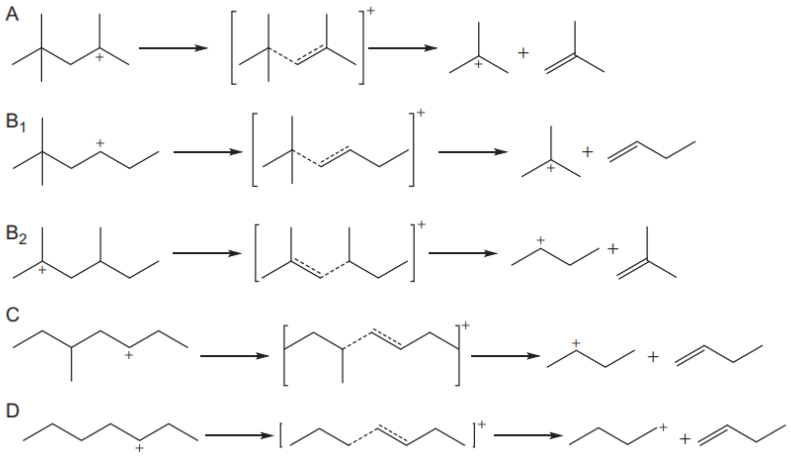

Figure 7: Reaction scheme of the different β-scission types. [24]

Type A β-scissions present the fastest rate out of all the cracking reactions since tertiary carbocations react and are formed. In cases where a secondary carbenium ion forms a tertiary carbenium ion the reaction is classified as type B1 and when the opposite occurs (tertiary to secondary) it is referred to as B2 β-scission. In type C β-scissions, a secondary carbenium ion is cracked resulting in another secondary carbocation and an alkane. Lastly, type D scissions start from a secondary carbocation and react into a primary carbenium ion. It is worth mentioning the consideration of type E β-scissions, introduced by Buchanan et al. [62], which imply the cracking

of a tertiary carbenium ion into a primary one, or vice versa. However, due to thermodynamic constraints related to the instabilty of the primary carbenium ion, type D and type E β-scissions most likely do not play any role on the overall cracking yield.

The reaction rates of all the mentioned reactions depend heavily on the reacting molecule structure as well as the nature of the formed products. Table 3 displays the different composite activation energies, which accounts for both the protonation and elementary reaction steps, for the two types of skeletal rearrangements in addition to the different β-scission types. As expected, reactions involving two tertiary carbenium ions present the lowest activation energy within each reaction family due to their high stabilities.

Table 3: Composite activation energies (ΔHprot+Eact) estimated by a regression on the experimental data with n-octane over Pt/CBV-760. [57]

	Alkyl Shift (kJ/mol)	PCP branching (kJ/mol)	β-scission (kJ/mol)
(s;s)	16.7 (±0.1)	45.6 (±0.1)	79.2 (±0.6)
(s;t)	14 (±2)	39 (±5)	64 (±4)
(t;s)			55 (±1)
(t;t)	8 (±3)	31 (±2)	34 (±2)

The relative rate of all reaction types is presented next, in decreasing order: type A_{isom} > type $A_{cracking}$ > type B_{isom} > type $B1_{cracking}$ ≈ type $B2_{cracking}$ > type $C_{cracking}$ > type $D_{cracking}$. It can be concluded that the skeletal rearrangement reaction will be followed by cracking in a consecutive way. This claim is confirmed by analyzing the product distribution obtained in the hydrocracking of *n*-decane over 0.5 wt% Pt/HUSY catalyst (Figure 8) [24] where it is possible to observe that for low conversions mostly monobranched isomers are obtained by PCP branching, followed by isomerization to dibranched species and only small amount of cracking products are detected. When tribranched isomers start to appear they are quickly cracked into lighter compounds, which means that these species barely contribute to the overall outlet composition. With increasing conversion, cracking products become more dominant while monobranched and dibranched species start to decrease given that they are isomerized into higher branch molecules and subsequently cracked. [63]

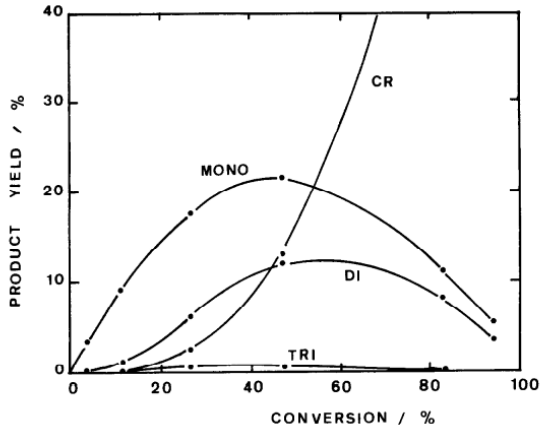

Figure 8: Distribution of monobranched (MONO), dibranched (DI), tribranched (TRI) isomers and cracking products (CR) for n-decane hydrocracking, over Pt/USY, as function of conversion. [63]

Overall, the hydrocracking reaction is exothermic, as the heat produced by the exothermic hydrogenation reactions is superior to the heat consumed by the endothermic cracking reactions. [44]

2.2.2 Cycloalkanes

The hydrocracking mechanism of cycloalkanes is the same as the one considered for alkanes. Firstly, the molecule is dehydrogenated on metal sites, followed by protonation into cabenium ion and will then undergo isomerization and cracking reactions on acid sites. Skeletal rearrangements can happen via intraring alkyl shifts, which can lead to the change of relative positions of the substitutes on the ring or to an expansion/contraction of the ring without changing the branching degree, as shown in Figure 9. Cyclic PCP branching also occurs, resulting an increase or decrease on the molecule branching degree. The cracking reactions can occur via endocyclic or exocyclic β-scissions, as represented in Figure 10.

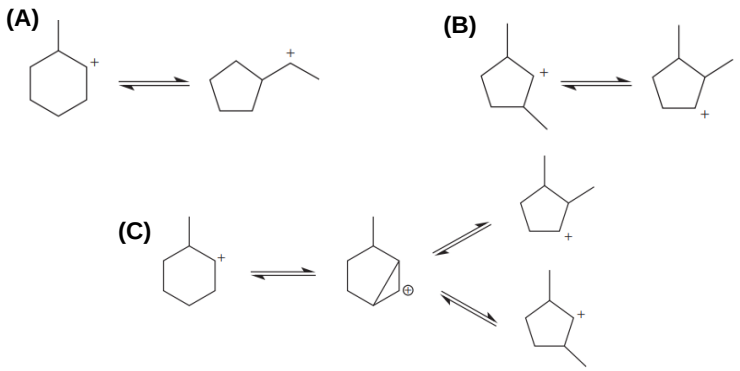

Figure 9: Reaction scheme for cycloalkane isomerizations: (A) Intraring alkyl shift with ring contraction without altering branching degree. (B) Intraring alkyl shift with change in branching degree and (C) cyclic PCP branching with ring contraction/expansion. [64]

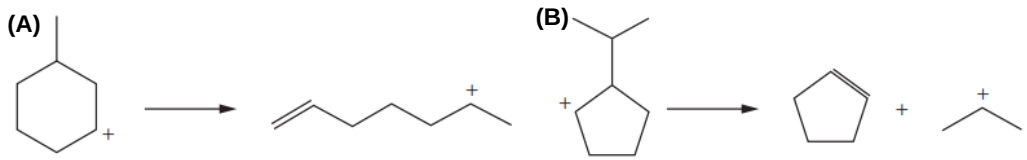

Figure 10: Reaction scheme for cycloalkane (A) endocyclic β-scision and (B) exocyclic β-scission. [64]

Table 4 shows the composite activation energies for both isomerization and cracking reactions of alkanes and naphthenes, which are dependent on the type of carbenium ion that intervenes in the reaction, decreasing with the increase in ion stability.

Table 4: Composite activation energies ($\Delta H_{prot}+E_{act}$) estimated by a regression on the experimental data with n-butylcyclohexane, over Pt/USY. [54]

	Alkyl Shift (kJ/mol)	Intraring Alkyl Shift (kJ/mol)	PCP branching (kJ/mol)	Cyclic PCP branching (kJ/mol)	Acyclic β-scission (kJ/mol)	Exoyclic β-scission (kJ/mol)	Endocyclic β-scission (kJ/mol)
(s;s)	15	25 (±2)	42	40 (±1)	68	76 (±1)	56 (±1)
(s;t)	14	21 (±3)	35	32 (±6)	55	57 (±7)	37 (±2)
(t;s)					53	56 (±5)	39 (±2)
(t;t)	10	Not estimated	30	27 (±3)	28	22 (±3)	31 (±7)

The rates of the above-mentioned elementary reactions are in the same order of magnitude of the corresponding reactions involving linear alkanes. Even though the composite activation energy for endocyclic β-scission is smaller than the ones for acyclic and exocylic reactions, the rate for β-scission between two carbon atoms of the naphthene ring is considerably slower because of a much lower pre-exponential factor [24][64]. This was demonstrated by Brouwer and Hogeveen by studying β-scission of one linear alkane and its corresponding cycloalkane (2,4,4-trimethylpentyl and 2,4,4-trimethylcyclopentyl, respectively). The authors justify this with the fact that in a linear alkane, there is free rotation around the α-carbon which results in a very efficient orbital overlap in the transition state of the reaction. Given the cyclic structure present in the naphthene molecule, there is little to no orbital overlap in the transition state meaning that the reaction is not likely to proceed [14][65]. Because of this, endocyclic β-scissions are not likely to occur, resulting in lack of cracking products for cycloalkanes with low carbon numbers, hence why the reaction network of a given naphthene will always be less extensive when compared to the reaction network of an alkane with the same carbon number.

Unlike what is observed in alkane hydrocracking, where only small amounts of tribranched species appear as products due to the fast type A β-scission (represented in Figure 8), in cycloalkane hydroconversion, the tribranched species are desorbed from the acid site without undergoing cracking and are detected as tribranched isomers in the reactor effluent.

2.2.3 Aromatics

Aromatic molecules possess special properties and stability when compared with other hydrocarbons due to their de-localized π-electrons clouds. Consequently, the hydrocracking reaction network of aromatic molecules is different in comparison to saturated hydrocarbons, as aromatic molecules can react directly to both metal and acid sites.

Aromatic compounds can be hydrogenated on metal sites, after which they will undergo the same elementary reactions as alkanes and cycloalkanes. Figure 11 shows the hydrogenation reaction of toluene which results in methylcyclohexane and isomers and will be followed by the classical bifunctional mechanism reactions mentioned in chapter 2.2.2. [66][67]

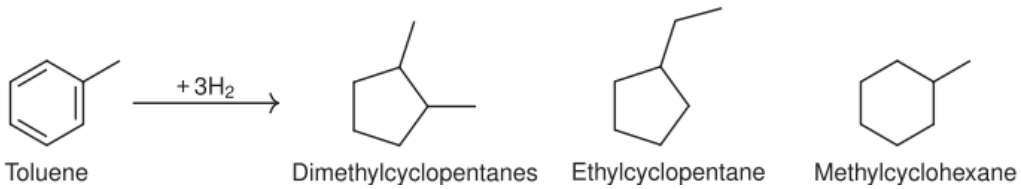

Figure 11: Reaction scheme of toluene hydrogenation.

Alternatively, aromatic molecules can adsorb directly to the catalyst acid sites where they are protonated, yielding aromatic carbenium ions which will then undergo further reactions. Similarly to alkanes and cycloalkanes, the aromatic elementary reactions can be differentiated into two groups: isomerization (or skeletal rearrangements, see Figure 12) and cracking, see Figure 13. Skeletal rearrangements can occur via alkyl shift, where the branching degree of the molecule is unchanged, or by transalkylation, where the branching degree of both reacting molecules is altered. The cracking reactions occur through dealkylation, where the alkyl group is separated from the aromatic carbenium ion.

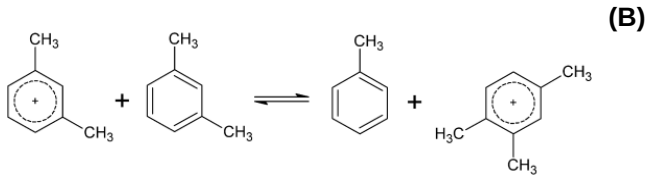

Figure 12: Reaction scheme of aromatic alkly shift. [68]

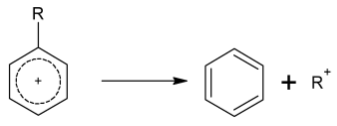

Figure 13: Reaction scheme for aromatic exocyclic β-scission. [68]

Due to the added reactions that can occur on acid sites without prior hydrogenation, the reaction network of aromatic molecules is more extensive compared to alkanes/cycloalkanes with similar carbon number and thus, more complex to understand. The direction of the aromatic molecules transformation strongly depends on the catalyst used, mainly on the strength of its acid sites but also on process conditions [67]. Work by Silva and coworkers [59] showed that the

addition of platinum decreased the rates of transalkylation and dealkylation on the transformation of ethylbenzene over Pt-HMOR catalyst [69].

Based on experimental results of ethylbenzene dealkylation/xylene isomerization over Pt/H-ZSM-5 catalyst [68], Toch and coworkers were able to obtain the activation energies for all the previously mentioned reaction families, as shown in Table 5. Dealkylation shows the highest activation energy due to the C-C bond cleavage between the alkyl group and the aromatic ring.

Table 5: Activation energies estimated through single-event kinetic model for ethylbenzene dealkylation/xylene isomerization, over Pt/H-ZSM5. [68]

	Alkyl Shift (kJ/mol)	Transalkylation (kJ/mol)	Dealkylation (kJ/mol)	Hydrogenation (kJ/mol)
Aromatic Carbenium Ion	134 (±2)	125 (±2)	194 (±2)	73 (±1)

Toch and coworkers [68] were also able to reach the relative importance of the reaction families: $R_{alkyl\ shift} > R_{dealkylation} > R_{transalkylation} > R_{hydrogenation}$. Observing Table 5, it is possible to see that the order of the activation energy is different: $R_{dealkylation} > R_{alkyl\ shift} > R_{transalkylation} > R_{hydrogenation}$. This difference is due to different entropy gains of the transition state in both reactions resulting in a much higher pre-exponential factor for the dealkylation reaction.

2.3 Hydrocracking regime: Ideal vs Non-Ideal Hydrocracking

Ideal hydrocracking is a special regime of bifunctional hydrocracking where the metal catalyzed reactions ((de)hydrogenation) are quasi-equilibrated while the reactions that occur on acid sites are rate-determining [4][70]. It can be observed when the metal function of the catalyst is strong enough to ensure a rapid desorption of the main products that are formed on the acid sites. In cases where the reactions that occur on acid sites are relevant to the overall rate of the hydrocracking reaction, the regime of non-ideal hydrocracking is observed. Ideal hydrocracking can be identified by two indicators: pressure impact on conversion and the independence of isomer yield regardless of process conditions, both of these markers will be further explored in this section.

The mechanism for the conversion of an *n*-alkane over a bifunctional catalyst can be used to understand one of the most salient features of ideal hydrocracking: maximum isomer yield. [70] After dehydrogenation on metal sites, the alkane is diffused into the Brønsted acid sites upon protonation into alkyl-carbenium ion undergoing type B isomerization reactions instead of slow β-scissions, due to higher composite activation energy, resulting in the change of the branching degree of the molecule. The recently formed monobranched isomer will rapidly desorb from the acid site due to strong hydrogenation metal function and the yield of this species will increase until the thermodynamic equilibrium between the protonation step and acid catalyzed reactions is achieved. Following this, the molecule can react through type B isomerization (increasing branching degree and producing dibranched isomers), or it can be cracked through type C β-scission, which is less likely. If the metal function has enough hydrogenation activity, a similar mechanism can be applied for dibranched isomers. With the increase in branching degree, tribranched isomers are formed, and will undergo cracking reactions since, as can be seen from Table 3, the composite activation energies for PCP branching and β-scission reactions between two tertiary ions are similar. At this conversion, the n-alkane isomer yield is maximum. Under ideal hydrocracking regime, a characteristic relationship between isomer yields and alkane conversion can be observed. [14]

Given the fact that type B skeletal rearrangements tend to occur near the central carbon atom of the molecule and that higher branched ions are more stable, the aforementioned cracking reactions will also occur near the center of the carbon chain resulting in higher yields of cracking products with j carbon atoms, where j represents half of the carbon number of the original octane. This results in a characteristic bell-shaped curve which is depicted in Figure 14 (curve Pt/Ca-Y). In the same figure, it can also be observed a non-symmetrical carbon number distribution (curve Co-Mo-S/SiO_2-Al_2O_3) which corresponds to non-ideal regime, where the larger primary cracking products will undergo secondary β-scissions because of the slow desorption step. Lastly, the curve SiO_2-Al_2O_3-ZrO_2 represents the extreme case of catalytic cracking where the desorption of species from the acid sites is really slow, leading to consecutive elementary reactions on a single site resulting in a significant amount of cracking products with low carbon number. [13][14]

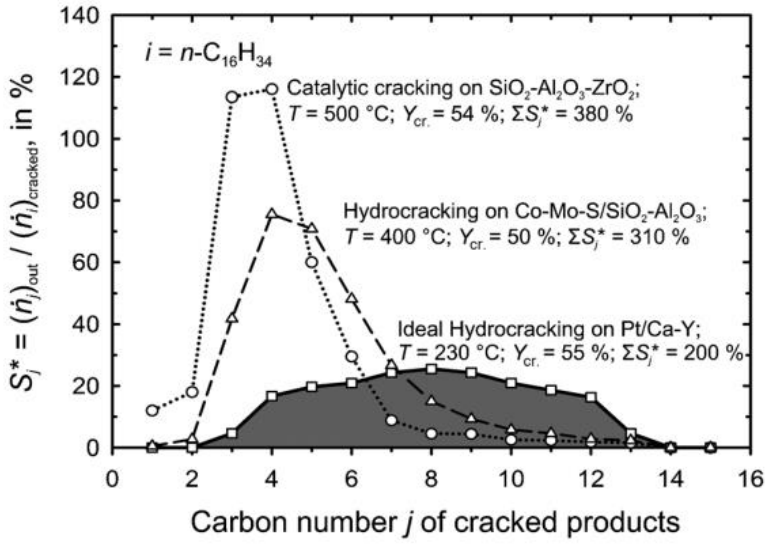

Figure 14: Molar distribution of cracking productions from n-hexadecane, for catalyst with different hydrogenation components. [14]

2.3.1 The influence of metal/acid site ratio on hydrocracking regime

The metal/acid site ratio is a key controlling parameter over the hydrocracking regime and depends on the concentration, metal site activity, strength and the distance between the two types of active sites. This parameter is responsible for the stability, activity and selectivity of the catalyst.

One of the ways to control whether ideal or non-ideal hydrocracking occurs is by altering the effective metal to acid site ratio. Degnan and Kennedy [71], used higher loadings of metal, which generally means stronger metal function, leading to the quasi-equilibrium of the metal catalyzed reactions, resulting in ideal hydrocracking.

Figure 15 plots the maximum isomer yield of *n*-heptane, over Pt/Al_2O_3 with various Pt loadings at 350 °C, 2.8 MPa and a hydrogen-to-hydrocarbon ratio of 5.36. It can be seen, that when metal content is lower than 0.6 m^2 Pt/g of zeolite, the maximum isomer yield changes drastically with the change in metal content since lower platinum loading leads to slower alkane diffusion to metal sites, allowing for multiple reactions of the alkane molecule on multiple acid sites, resulting in excessive cracking and possible deactivation of the catalyst [24] (non-ideal hydrocracking). However, for higher metal/acid ratios, it can be observed that the slope of the curve tends towards zero meaning that the overall reaction rate is determined by the acid-catalyzed reactions and thus ideal hydrocracking regime is achieved for higher platinum loading.

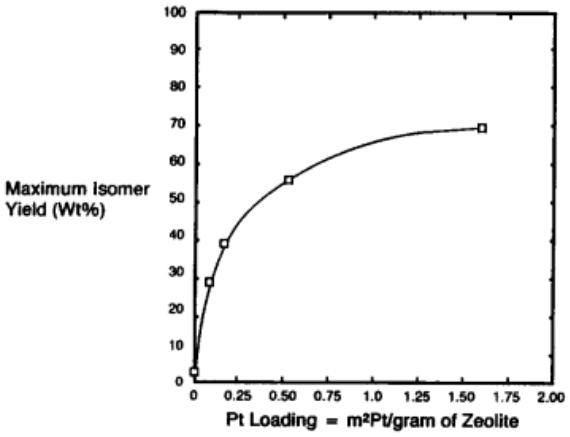

Figure 15: Maximum isomer yield of n-heptane as function of metal to acid site ratio (T = 350 °C, P = 2.8 MPa, H_2/HC molar ratio = 5.36). [71]

The catalyst used in the experiments by Degnan and Kennedy [71] had similar dispersion values, meaning that the isomer yields obtained with different platinum loadings can be related since the fraction of exposed platinum throughout all experiments is comparable.

Alvarez and coworkers followed the ratio of final/initial activity of Pt/HY catalysts in the transformation of *n*-decane, at 200 °C, 101 kPa (see Figure 16) [49]. The deactivation of the catalyst depends on this ratio, and it was found that increasing metal/acid site ratio (n_{Pt}/n_{H+}) lead to an increase in the final/initial activity ratio. For (n_{Pt}/n_{H+}) values above 0.1, the ratio between final and initial activities remained constant at 1.

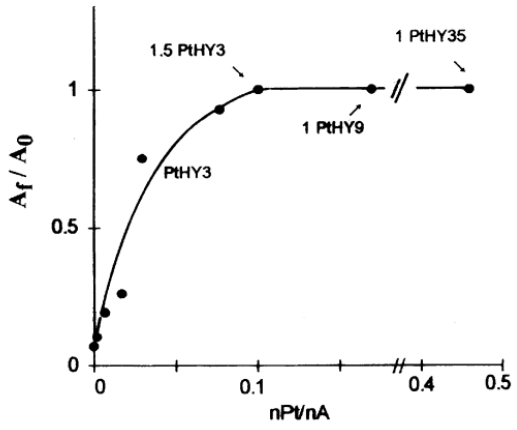

Figure 16: Ratio of the final/initial activities of Pt/HY catalysts in n-decane transformation, as function of metal/acid site ratio (T = 200 °C, P = 1 bar, H_2/HC molar ratio = 9). [49]

In the same work, Alvarez et al [49] found that increasing metal/acid site ratio results in lower initial activity and higher ratio of isomerized/cracked products. Table 6 shows the influence of the metal-to-acid site ratio on the activity, stability and reaction scheme of the *n*-decane transformation.

Table 6: Influence of different metal to acid site ratio on activity, stability and reaction scheme of n-decane hydrocracking (T=200°C, P = 1 bar, H_2/HC molar ratio=9). [49]

n_{Pt}/n_{H+}	< 0.03	> 0.03; < 0.10	> 0.10
Activity	Low	Maximal	Maximal
Stability	Low	Average	Perfect
Reaction Scheme	$nC_{10} \rightleftharpoons M$ $nC_{10} \rightleftharpoons B$ $nC_{10} \rightarrow C$	$nC_{10} \rightleftharpoons (M, B) \rightarrow C$	$nC_{10} \rightleftharpoons M \rightleftharpoons B \rightarrow C$

When the metal to acid site ratio is low (< 0.03), the number of available Pt sites is insufficient to feed all the acid sites with intermediate alkenes, meaning that the dehydrogenation step will rate-determining for the hydrocracking over bifunctional catalyst. Given this, non-ideal hydrocracking occurs, since the occurrence of multiple reactions on a single acid site is expected, resulting in all isomerization and cracking products to appear as primary products of hydrocracking. The formation of coke also occurs, which deactivates the catalyst.

Increasing the value of n_{Pt}/n_{H+} (> 0.03, < 0.10) improves the activity of the catalyst, until it is maximal, meaning that the quantity of available Pt sites is enough to feed all the acid sites with intermediate alkenes. In this case, the rate-determining step is the transformation of the alkenes on the acid sites. However, the distance between metal sites is still large enough for the occurrence of some consecutive acid-catalyzed reactions resulting in the formation of coke and consequent catalyst deactivation. In this case, non-ideal hydrocracking also occurs.

For high values of n_{Pt}/n_{H+} (> 0.10), the activity remains maximal while the distance between active sites is lowered, meaning that only one transformation of alkene intermediate will occur before hydrogenation thus approaching the ideal hydrocracking mechanism. Despite this, it was found that ideal hydrocracking occurs when the metal to acid site ratio is higher than 0.17 [49]. It is worth noting that too much Pt content might catalyze hydrogenolysis or induce pore blockage. [24]

2.3.2 The influence of operating conditions on hydrocracking regime

As mentioned in chapter 2.3.1, ideal hydrocracking is highly dependent on the metal to acid site ratio of the used catalyst however, operating conditions (temperature, pressure and hydrogen-to-hydrocarbon ratio) also impact the observed hydrocracking regime and catalyst activity. This means that a catalyst can be well balanced for a given set of operating conditions while exhibiting non-ideal hydrocracking upon a change in the process conditions.

Temperature

Higher temperatures favor non-ideal hydrocracking. Both the acid-catalyzed and dehydrogenation reaction rates increase with temperature meaning that at higher temperatures

both reaction rates will increase. However, the reactions that happen on acid sites have higher temperature dependence [13] meaning that with an increase in temperature the rate of these reactions will increase faster while the hydrogenation reactions will not be able to follow up, leading to more successive reactions on a single acid site and inducing a shift towards non-ideal hydrocracking. [71]

Pressure

Lower pressures favor non-ideal hydrocracking. An increase in pressure leads to an increase in hydrogen partial pressure and, consequently, the (de)hydrogenation rate. In ideal hydrocracking, thermodynamics control the (de)hydrogenation reactions and due to Le Chatelier principle, the hydrogenation reaction is favored, lowering alkane (and carbenium ions) concentrations at higher pressures. Since the concentration of carbenium ions is lowered with the pressure increase, the reaction rates of the acid-catalyzed reactions will also be reduced which leads to a decrease in conversion. [13]

However, when non-ideal hydrocracking regime is observed, the higher concentration of adsorbed alkanes will increase the (de)-hydrogenation rate leading to higher alkene (and carbenium ions) concentration given that the (de)-hydrogenation reactions is no longer in equilibrium, which increases the rate of the isomerization and cracking reactions that occur on acid sites. This means that in non-ideal hydrocracking regime, an increase in pressure (by adjusting hydrogen-to-hydrocarbon ratio) leads to higher conversions.

Figure 17 [5] shows the impact of pressure on *n*-alkane conversion over bifunctional catalyst [13]. It can be observed the different conversion dependence on pressure depending on if ideal or non-ideal hydrocracking is detected. In ideal hydrocracking, higher pressure leads to lower conversion while in non-ideal hydrocracking regime, an increase in pressure results in an increase in *n*-alkane conversion. This conversion dependence is used as clear way to identify the occurrence of ideal hydrocracking.

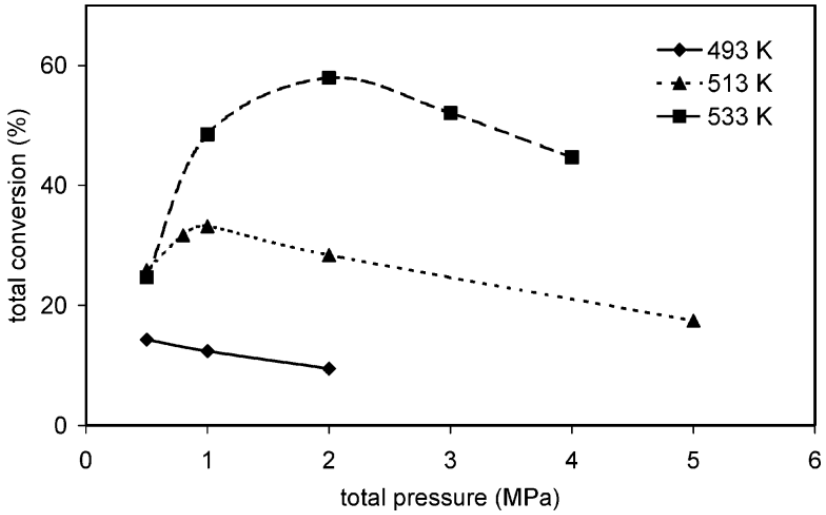

Figure 17: n-decane hydrocracking conversion as function of total pressure and the effect of temperature. (H_2/HC molar ratio of 200). [13]

Figure 17 also allows for the examination of the temperature effect on non-ideal hydrocracking. For a total pressure of 1 MPa, when the temperature is low (493 K) ideal hydrocracking is observed due to the conversion decrease with pressure increase however, at higher temperature (533 K) and same total pressure, the conversion dependence on pressure is now opposite, increasing with total pressure indicating non-ideal hydrocracking. This shows that, at the same pressure, higher temperatures lead to a shift towards non-ideal hydrocracking.

Hydrogen-to-hydrocarbon ratio

Higher hydrogen-to-hydrocarbon ratio favors non-ideal hydrocracking [13], however the effect of this parameter is smaller than the impact of temperature, pressure or carbon number. An increase in hydrogen-to-hydrocarbon ratio will increase the hydrogen concentration in the hydrocracking feed which will reduce the desorption rate of carbenium ions from acid sites, inducing a shift towards non-ideal hydrocracking due the occurrence of consecutive acid-catalyzed reactions. This desorption rate is lower due to the impact on the (de)hydrogenation equilibrium which is shifted towards the reactants due to higher hydrogen concentration [13]

Feedstock carbon number

Feedstocks with higher carbon numbers will favor non-ideal hydrocracking. Alkanes with higher carbon number have larger reaction networks. Since the number of acid-catalyzed steps increases faster with the carbon number than the (de)-hydrogenation reactions [13], so will the reaction rates of both reactions, resulting in the occurrence of successive isomerization/cracking reactions on acid sites, meaning that higher concentration of metal sites is needed to achieve ideal hydrocracking when using larger molecules. [72]

Understanding the transition between ideal and non-ideal regime is important for the hydrocracking process given that it affects not only the product distribution but also the catalyst stability. This transition is dependent on the quasi-equilibrium of the (de)hydrogenation reactions which can be achieved by altering the effective metal to acid site ratio (i.e changing metal loading) or by adjusting process conditions such as temperature, pressure, or hydrogen-to-hydrocarbon ratio. One of the ways to identify ideal hydrocracking is by observing the impact of pressure on the conversion of *n*-alkane, and the second way is to detect the characteristic curve of isomer yield as function of *n*-alkane conversion.

2.4 Hydrocarbon admixture impact on hydrocracking

The individual reaction network and mechanisms of different hydrocarbons that can be found in an industrial hydrocracking feed as well as the concept of ideal hydrocracking were introduced previously. In zeolite-based systems, the rates and product distributions are often determined by adsorption and diffusion properties inside the pores, which can be heavily impacted by the chemical properties of different molecules.

In this section, the interactions between different molecular species (*n*-alkanes, cycloalkanes and aromatics) will be studied in further detail as well as the impact that these interactions can have on conversion, product distribution and hydrocracking regime.

2.4.1 Alkane admixture effects

It has been reported in literature that *n*-alkanes with higher carbon number are more reactive. This means that, in general, hydrocracking of *n*-alkane with higher carbon chain is expected to have a negative impact on the conversion and isomer selectivity of smaller hydrocarbon. This effect can be explained by different phenomena: (1) Physisorption rate of *n*-alkanes increases with carbon number; (2) Protonation step is favored towards high chain alkanes since adsorption on acid sites is faster for heavier hydrocarbons and the formed carbenium ion stability also increases with carbon number; (3) *n*-alkanes with higher carbon number have more extensive reaction network which results in a larger number of elementary reactions on the catalyst acid sites, increasing the rate of hydrocracking reaction. [24][70][73]–[76]

Guisnet and coworkers [77] investigated the hydroisomerization of *n*-hexane over platinum catalyst on mordenite (PtHMOR) with small amounts of impurities added (5 %wt). *n*-hexane transformation was carried out under the pressure of 1 bar, a hydrogen/hydrocarbon ratio of 4 and temperature of 250°C. Two 0.3 wt% PtHMOR catalysts were used with Si/Al ratios of 8 (PtHMOR8) and 68 (PtHMOR68). The impact of adding *n*-alkanes to a pure *n*-hexane feed is shown in Figure 18.

The addition of *n*-pentane showed no change in activity of both catalysts. The inhibition effects of *n*-heptane and 2-methylhexane were dependent on the catalyst. For PtHMOR8, which has lower Si/Al ratio, deactivation was observed while for PtHMOR68, the introduction of other hydrocarbons seemed to have no impact on the activity of the catalyst. This difference in catalyst behavior indicates that PtHMOR8 is well-balanced only for the pure *n*-hexane feed. The introduction of *n*-heptane and 2-methylhexane also lowered the conversion of *n*-hexane.

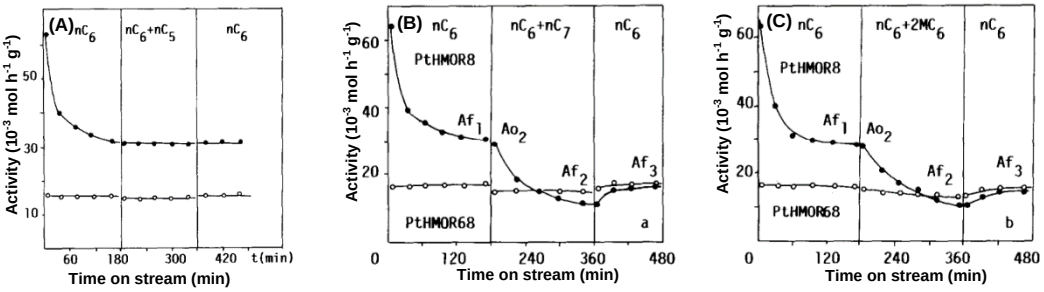

Figure 18: Influence of (A) n-pentane, (B) n-heptane and (C) 2-methylhexane on the hydroisomerization of n-hexane over PtHMOR8 and PtHMOR68 (T = 250°C, P = 1bar, H_2/HC molar ratio = 4). [77]

Similar results were obtained by Hollo et al. [76], who studied the hydroconversion of binary mixtures of *n*-hexane in *n*-pentane and *n*-heptane in *n*-hexane. The experiments were conducted at 210°C, with total pressure of 30 bar over 0.4% Pt/HMOR catalyst. In both cases, the presence of heavier alkane in the mixture lowered the reactivity of the lighter alkane compared to when the feed was pure.

Sánchez et al. [75] followed the conversion and isomer selectivity of the hydrocracking of binary mixture between nC_6 and nC_8 and compared the results to hydrocracking of the pure alkanes. The experiments were conducted at 330°C and 10 bar over 1 wt% Pt H-beta zeolite catalyst (Si/Al = 12.5) agglomerated with bentonite (PtBetaBent). It was observed that the reactivity of the *n*-alkanes increased with chain length (nC8 > nC7 > nC6) due to the increase stability of alkene intermediates with increase in carbon number. The conversion of *n*-heptane increased slightly when fed in equimolar mixture with a lighter alkane (*n*-hexane) and decreased when the equimolar mixture was done with *n*-octane. This behavior can be explained by the preferential adsorption of heavier alkanes and by the fact that the protonation step is favored towards hydrocarbons with higher carbon number. The combination of these two factors inhibits the adsorption of lighter alkanes thus reducing their conversion. In comparison to when it was fed pure, the conversion of *n*-octane increased when mixed with smaller alkanes. This effect was less noticeable for the equimolar mixture between *n*-octane and *n*-heptane since the difference in adsorption strength between the two components is smaller than in the case of *n*-octane/*n*-hexane mixture.

The addition of linear alkanes also led to negative impacts on the isomer selectivity. When fed in equimolar mixture with *n*-octane, the isomer selectivity of *n*-heptane was significantly lowered and no effect was observed when *n*-heptane was mixed with *n*-hexane. The more extensive reaction network of *n*-octane and the competitive adsorption for acid sites between intermediate molecules appear to be the reason for this reduction in isomer selectivity. Isomer selectivity of *n*-hexane remained similar when fed in mixture with *n*-octane however it was drastically lowered when *n*-hexane was co-fed with *n*-heptane. It is important to note that isomer selectivity is dependent on conversion. For every component, there is a conversion where the maximum isomer yield is reached, however if conversion increases past that point, the isomer yield will start decreasing. This was observed when *n*-heptane was fed in mixture with *n*-hexane

but also in both mixtures of *n*-octane, where conversion was increased but isomer selectivity was reduced.

Denayer and coworkers [78] investigated the hydroconversion of the mixture of *n*-heptane and *n*-nonane over 0.5 wt% Pt/Beta catalyst (Si/Al = 12.5), at 230°C and 4.5 bar of total pressure. The results obtained are in accordance with others previously reported since the conversion of *n*-nonane was preferential. The higher adsorption enthalpy of *n*-nonane compared to n-heptane, means that the heavier component has tendency to adsorb faster is one of the reasons for the observed differences in conversion. Other reason is the fact that *n*-nonane reacts faster than *n*-heptane on the acid sites due to its larger reaction network which result in higher number of possible carbenium ion transformations.

It can be summarized that the mixture of alkanes with varying carbon numbers has effects on both conversion and isomer selectivity. The introduction of lighter alkanes seems to have no negative impact on conversion. Alternatively, conversion of a given *n*-alkane in mixture with a heavier alkane will be decreased in comparison to when it is fed pure. Selectivity towards isomers is reduced with the addition of a hydrocarbon with smaller carbon chain while in cases where the added alkane is heavier, the effect on isomer selectivity can be negative or considered as negligible. In certain cases, the differences in adsorption strengths between *n*-alkanes can prove to be enough to disturb the metal/acid site ratio of the catalyst, inducing a shift in hydrocracking regime.

2.4.2 Cycloalkane admixture effects

As mentioned in subchapter 2.2.2, cycloalkane reaction mechanism is similar to the reaction scheme of linear alkanes. Cycloalkanes condense more easily at the catalyst than alkanes and their adsorption on acid sites is stronger as well [79]. Consequently, competitive adsorption on acid sites between alkanes and cycloalkanes is expected to occur. This effect is generally considered responsible for the observed impact of cycloalkanes on alkane conversion and isomer selectivity during hydrocracking.

Guisnet and Fouche [77] also studied the impact of co-feeding methylcylohexane on the hydrocracking of *n*-hexane, over two different catalysts (PtHMOR8 and PtHMOR68). In both cases, the introduction of the cycloalkane resulted in catalyst activity decrease, as shown in Figure 19. This inhibitory effect was stronger than the one observed when linear alkanes (*n*-heptane and 2-methylhexane) were introduced as impurities. The reason for stronger inhibition effect of cycloalkanes is the competitive adsorption for acid sites between the cyclic molecules and formed hexenes. Upon protonation, methylcyclohexane results in a tertiary carbenium ion which is more stable than the products from hexene protonation, meaning that the former reaction is favored.

Similarly to the experiments with linear alkanes, the impact of methylcyclohexane on *n*-hexane hydrocracking was more noticeable when the more acidic catalyst (PtHMOR8) was used.

It should be mentioned that although PtHMOR68 catalyst appeared to remain well-balanced with the addition of *n*-heptane or 2-methylhexane, the activity reduction observed with the introduction of methylcyclohexane indicates that rebalancing of the catalyst is needed. Upon reintroduction of *n*-hexane as pure feed different behaviors were observed. With PtHMOR68, activity increased until becoming practically equal to the initial value, meaning that no catalyst deactivation occurred. Alternatively, when PtHMOR8 was used, the catalyst was deactivated most likely due to the formation of coke generated by cracking reactions. [75][77]

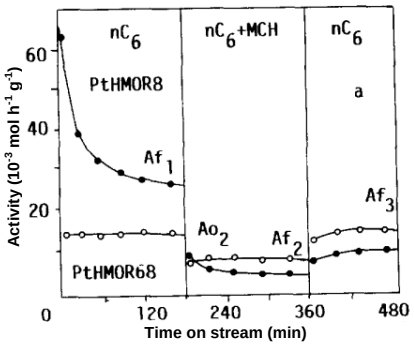

Figure 19: influence of methylcyclohexane on the hydroisomerization of n-hexane over PtHMOR8 and PtHMOR68. (T = 250°C, P = 1bar, H_2/HC molar ratio = 4). *[77]*

Hydrocracking of *n*-hexane and cyclohexane mixture over 0.5 wt% Pd-H-Mordenite catalyst was investigated by Hatcher [34]. Several experiments were done with a molar mixture of 56% cyclohexane and 44% *n*-hexane, with temperatures ranging from 315 to 340 °C. Experimental results showed that cyclohexane was preferentially converted in the mixture and the conversion of *n*-hexane was lower than when it was fed as pure component. Walter et al. [80] also investigated the hydrocracking of equimolar mixture of *n*-hexane and methylcyclohexane over alumina supported Pt, Ir and Ru catalysts. The conversion of *n*-hexane was lowered by the addition of methylcyclohexane. Alternatively, the conversion and isomer selectivity of methylcyclohexane was not affected by the presence of *n*-hexane. Through dehydrogenation of methylcyclohexane, toluene was detected in product outlet only when Pt catalyst was used, due to its higher hydrogenolytic activity when compared with Ir and Ru catalysts [80]. In both investigations (Hatcher[30]; Walter et al.[71]), The observed impact of methylcyclohexane on *n*-hexane hydrocracking was explained by the competitive adsorption between reactants [34].

By examining the reactivity of binary and ternary mixtures of alkanes (nC_6, nC_7 and nC_8) and cyclohexane, Sánchez and coworkers [75] were able to assess the effects of different hydrocarbons on conversion and isomer selective of *n*-alkane hydrocracking, over 1 wt% Pt/BetaBent catalyst. The conversion of all *n*-alkanes was lower when fed in mixture with cyclohexane, due to its preferential adsorption on the zeolite. The selectivity to *n*-alkanes isomers also decreased when fed in mixtures with cycloalkane. It was found that cyclohexane conversion was depended not only on temperature but also on whether the mixture was binary or ternary. Cyclohexane conversion increased when fed in mixture with *n*-alkanes and was found to be maximum when binary mixtures were used.

The hydroisomerization of a hydrocarbon mixture containing 65% *n*-hexane, 15% *n*-heptane and 20% cyclohexane (wt%), over different zeolite platinum catalysts, was investigated by Jiménez and coworkers [81]. Pt/USY and Pt/Beta catalysts achieved higher selectivity towards isomerization, while Pt/Mordenite catalysts were found to be more selective towards cracking products. It was also found that the reactivity sequence between hydrocarbons varied with the zeolite that was used. As observed by Sánchez et al. [75], naphtene conversion was temperature dependent however, it was found that selectivity towards cyclohexane dehydrogenation depended on the catalyst used. USY and Ferrite zeolites favored this reaction, while Beta zeolites were found to be more selective towards isomerization into methylcylopentane.

In the same work [81], the reactivity of each feed component was compared between binary and ternary mixtures over Pt/Mordenite catalyst. The partial pressures of *n*-hexane and *n*-heptane increased in the feed where no cyclohexane was present. As found in other investigations, this effect can be explained by the preferential adsorption of the cycloalkane on the catalyst acid sites.

The impact of co-feeding methylcyclohexane on *n*-octane hydrocracking, over Pt/HUSY catalyst was investigated by Korica et al. [72]. Experiments were conducted with temperatures ranging between 250 °C and 350 °C, pressures of 10 and 20 bar and equimolar mixture. The used catalysts had different platinum loadings (0.5 wt%, 0.1 wt%, 0.07 wt% and 0.04 wt%) , where 0.5 wt% and 0.1 wt% Pt loadings were confirmed to ensure equilibrated (de)hydrogenation of *n*-octane. It was found that the addition of methylcyclohexane did not impact the *n*-octane conversion or isomer yield over well-balanced catalysts. Over poorly-balanced, *n*-octane conversion was lowered by the presence of methylcyclohexane with this effect being more noticeable at lower metal content. In these conditions, *n*-octane isomer yield was reduced and the selectivity towards multibranched isomers increased.

The conversion of methylcyclohexane (lower carbon number) was not affected by the presence of *n*-octane (higher carbon number) over well-balanced catalysts, which indicates that preferred adsorption on acid sites did not occur to any significant extent. It can thus be said that the kinetically relevant steps are the ones that occur on metal sites of the catalyst [72]. The preferential adsorption of methylcyclohexane over *n*-octane on metal sites leads to a reduction in metal/acid sites ratio, resulting in decrease in conversion of *n*-octane. The decrease in available metal sites increases selectivity towards multibranched *n*-octane isomers since it forces consecutive reactions on acid sites, which could lead to a shift from ideal to non-ideal behavior.

In order to understand how the impact of cycloalkanes on *n*-alkane hydrocracking varies with carbon number, hydroconversion of *n*-octane/*tert*-butylcyclohexane and *n*-decane/methylcyclohexane mixtures, over Pt/HUSY catalysts was also investigated [82]. It was observed that *tert*-butylcyclohexane admixture reduced *n*-octane conversion and isomer selectivity, over both well- and poorly-balanced catalyst. This effect had already been detected with methylcyclohexane in previous investigations due to the preferential cycloalkane adsorption on metal sites [72]. However, the cycloalkane admixture impact was stronger with *tert*-

butylcyclohexane, as shown in Figure 20, given its preferred adsorption on metal sites, but also because of the preferred physical adsorption to the zeolite due to its higher carbon number.

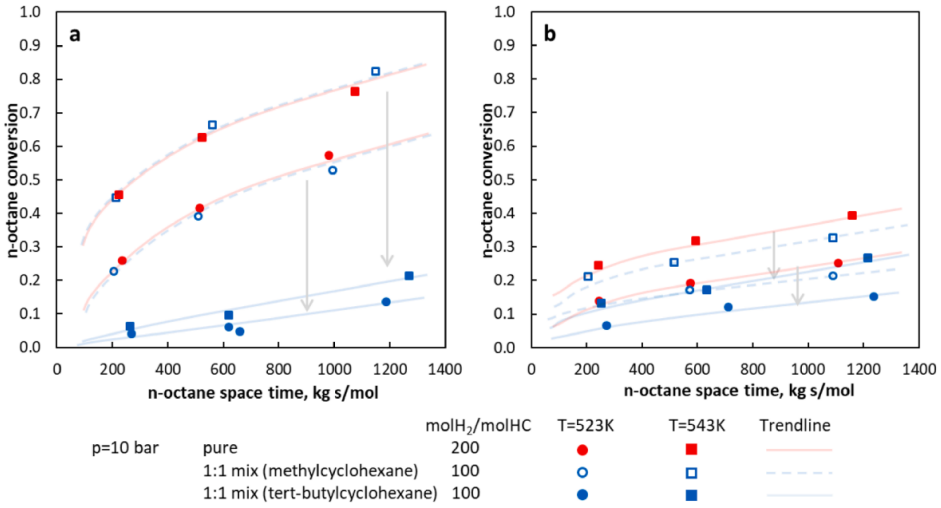

Figure 20: Influence of methycyclohexane and tert-butylcyclohexane on n-octane hydrocracking over (A) 0.3 wt% Pt/HUSY and (B) 0.07 wt% Pt/HUSY (T = 250 to 270 °C, P = 1 bar). [82]

Methylcyclohexane did not affect *n*-decane conversion or isomer yield over well-balanced catalyst which indicates that the cycloalkane preferential adsorption on metal sites was not strong enough to shift the hydrocracking regime to non-ideal. Alternatively, *n*-decane conversion decreased with methylcycloalkane admixture over the poorly-balanced catalyst, as shown in Figure 21. However, this reduction was more pronounced than the reduction in *n*-octane conversion when methylcyclohexane was co-fed [72] (Figure 20-A and Figure 21-B), likely due to the higher reactivity of *n*-decane coupled with the preferential adsorption of methylcyclohexane on acid sites. The impact of cycloalkane admixture on the hydroconversion of *n*-alkane with higher carbon number, becomes weaker with increase in carbon number difference. Methylcyclohexane conversion was lowered when fed in mixture with *n*-decane, due to the stronger physical adsorption of the linear alkane.

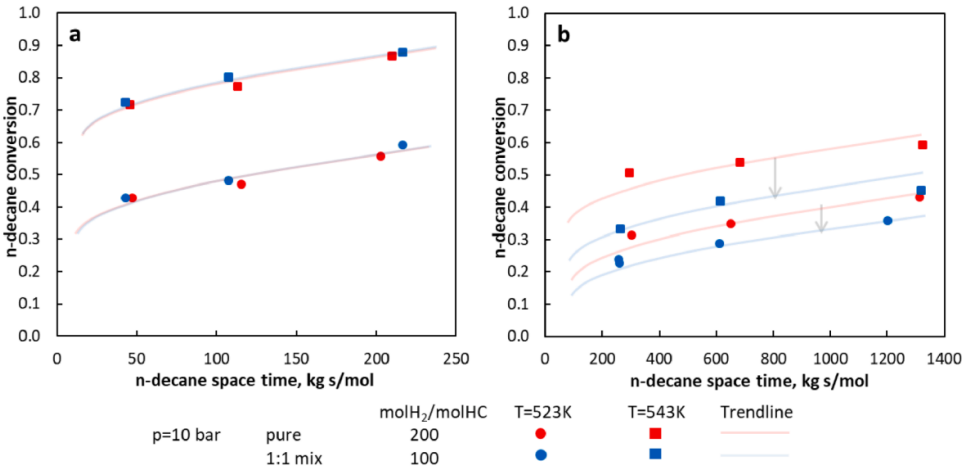

Figure 21: Influence of methycyclohexane on n-decane hydrocracking over (A) 0.3 wt% Pt/HUSY and (B) 0.07 wt5 Pt/HUSY (T = 250 to 270 °C, P = 1 bar). [82]

As seen, the impact of co-feeding cycloalkanes on *n*-alkane hydrocracking, can be explained by competitive adsorption between reactants over metal and acid sites. This competitive adsorption impacts the metal/acid site ratio of the catalyst, potentially leading to a shift in hydrocracking regime. This means that, similarly to *n*-alkane mixtures, a catalyst deemed as well-balanced for hydrocracking of a pure component, may become poorly balanced when different hydrocarbons mixtures are used. The difference in molecule size between alkanes and cycloalkanes also is important when determining the cycloalkane admixture impact. The effects on *n*-alkane conversion and isomer selectivity will be maximum when the carbon number of both molecules is the same, being gradually reduced with the increase in carbon number difference between *n*-alkane and cycloalkane.

2.4.3 Aromatic admixture effects

The reaction network of aromatic molecules is unique due to its ring structure. As mentioned in subchapter 2.2.3, aromatics can either be hydrogenated to cycloalkanes on metal sites, upon which they will undergo the same elementary reactions as naphtenes, or they can adsorb on the acid sites, being subject to disproportionation and dealkylation reactions. Aromatic compounds exhibit stronger adsorption due to the higher availability of π electrons, and to the fact that the formed carbenium ions are more stable, which is one of the reasons for the impact of aromatic admixture effects on *n*-alkane hydrocracking. Another reason for these effects is the shape selectivity that results from the adsorption of bulkier aromatic molecules to the catalyst surface, potentially blocking the accessibility to other active acid sites.

Guisnet and coworkers [77] studied the hydroisomerization of *n*-hexane over platinum catalyst on mordenite (PtHMOR) with the addition of aromatic molecules. The impurities added were toluene (5 wt%) and 1-methylnaphtalene (1 wt%). *n*-hexane transformation was carried out under the pressure of 1 bar, a hydrogen-to-hydrocarbon ratio of 4 and temperature of 250°C. Two samples of mordenite were tested, one with a Si/Al ratio of 8 and the second one with a ratio of 68. The results obtained are shown in Figure 22.

The addition of toluene reduced the activity of both catalysts and only impacted the stability of PtHMOR8, since upon reintroduction of *n*-hexane as pure feed, the catalyst activity of PtHMOR68 approached values similar to the ones obtained initially. Even in lower concentration, 1-methylnaphtalene had a stronger inhibitory impact on both catalysts activity and stability, likely due to its higher carbon number and size. The *n*-hexane activity reduction with impurities is due to the preferential adsorption of aromatic molecules over the catalyst acid sites [77][83]. As observed, it was expected the inhibition effect to increase with aromatic acidity, since the carbenium ion formed by protonation of 1-methylnaphtalene is more stable than the one obtained from toluene. Isomerization/cracking (I/C) ratio of *n*-hexane was also analyzed, and results showed that, depending on used catalyst, I/C ratio increased (PtHMOR68) or decreased

(PtHMOR8). This indicates that upon addition of aromatic molecules, the catalysts no longer remains well-balanced.

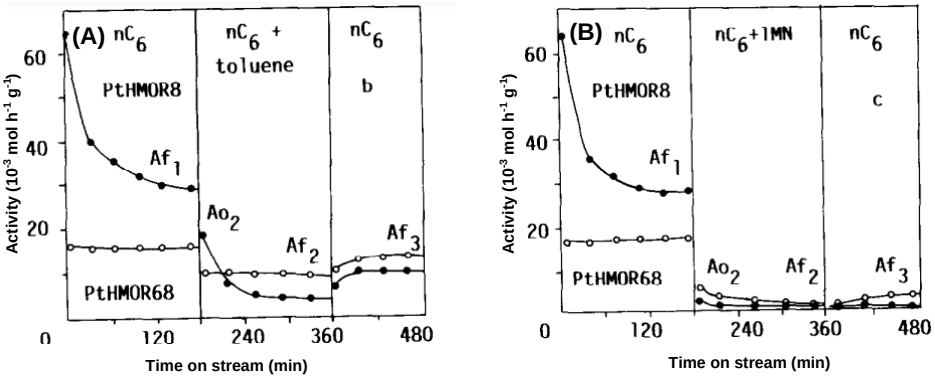

Figure 22: Influence of (A) toluene and (B) 1-methylnaphtalene on the hydroisomerization of n-hexane over PtHMOR8 and PtHMOR68 (T = 250 °C, P = 1 bar, H2/HC molar ratio = 4). [77]

Chen et al. [84] investigated the hydroisomerization of *n*-hexane isomers over Pt-Mordenite, with 20% of benzene. Experiments were run at 275 °C, 0.76 MPa and with a hydrogen-to-hydrocarbon ratio of 10. The introduction of benzene inhibited the conversion of *n*-alkanes and changed the relative reactivities between *n*-hexane isomers, as shown in Figure 23. Benzene leads to a decrease in conversion across all isomers, explained by acid site suppression caused by the preferential adsorption of the aromatic molecule. When fed pure, 2,3-dimethylbutane was the most reactive alkane however, upon introduction of benzene, *n*-hexane became the most reactive. This effect is explained by the difference between kinetic diameters of *n*-hexane and branched isomers, indicating that toluene limits intrapore diffusion of the paraffins. [84]

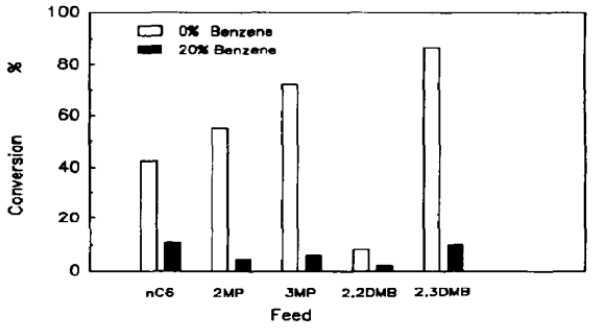

Figure 23: Comparison of n-hexane isomer reactivities with benzene admixture. (T = 275 °C, P = 0.76 MPa). [84]

Chen and coworkers also studied the impact of different aromatic co-feed on *n*-hexane hydroisomerization, over 0.6 wt% Pt/Mordenite [85]. The aromatics components used were benzene, toluene, *p*-xylene and mesitylene and their conversions increased when fed in mixture with *n*-hexane. The experimental conditions were the same as the ones used in prior investigation [84]. Hydroisomerization activity of *n*-hexane decreased with the addition of aromatic molecules, due to competitive adsorption between intermediate molecules for active acid sites, seen in Figure 24. It can also be observed in Figure 24, an increase in *n*-hexane isomer formation rate between *p*-xylene and mesitylene. Again, the difference in kinetic diameter of the molecules is responsible

for this effect which, in this case, is beneficial for the isomerization of *n*-hexane since the bigger size of mesitylene limits its accessibility to the pore channels and active sites.

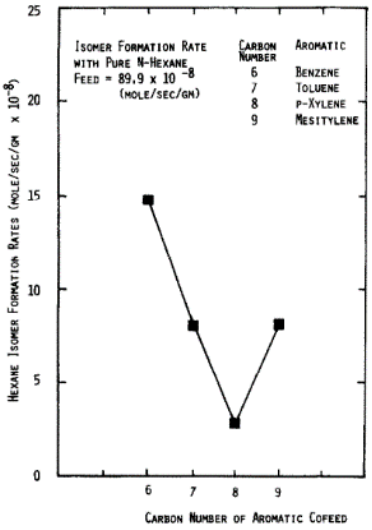

Figure 24: Influence of aromatic carbon number on n-hexane reaction rate, over 0.6% Pt/Mordenite (T = 275 °C, P = 0.76 MPa). [85]

From both investigations [84][85], it can be concluded that the aromatic impact is caused not only by acid active site suppression, but also due to pore blockage induced by the aromatic components.

Sánchez and coworkers [66] studied the impacts of benzene on the hydroisomerization of a mixture of *n*-heptane and *n*-octane [75]. It was observed that the partial conversions of *n*-alkanes increased when fed in ternary mixture with benzene. Isomer selectivity of *n*-heptane/*n*-octane was lower than what was observed when they were fed in binary mixture without benzene. Although aromatic compounds seem to inhibit the conversion of *n*-alkane, in this case the opposite was observed, since the presence of benzene promoted the conversion of the paraffins, which is quite unique.

The hydrocracking of *n*-hexadecane in the presence of benzene and naphthalene, over 0.5 wt% Pt-Pd/WO3-ZrO2 was assessed by Busto et al. [86]. The experiments were conducted at 225 °C, 20 atm with a hydrogen-to-hydrocarbon ratio of 10. Both aromatic compounds decreased the hydrocracking activity however, the effect of naphthalene was less pronounced. It was found that benzene reduces cracking selectivity because it adsorbs preferentially on the catalyst strong acid sites (zeolite cages), where the cracking to light cases occurs thus inhibiting said reaction [86]. Busto and coworkers concluded that the presence of benzene, in low concentrations, could be beneficial to the selectivity of the reaction however, benzene content higher than 0.5 % was found to decrease catalyst activity without improving the reaction selectivity.

In the work of Tailleur and Nascar [87], the effects of 1-methylnaphtalene over *n*-hexadecane hydrocracking were studied. Experiments were conducted at temperatures ranging

from 340 °C to 360 °C, pressure of 81 bar and hydrogen-to-hydrocarbon ratio of 4, over WNiPd on CeY-alumina support. The conversion of *n*-hexadecane decreased with the introduction of 15% and 30% 1-methylnaphtalene to the feed, due to the preferential adsorption of the aromatic molecule to the acid sites of the catalyst. Similarly to what was observed in the investigation by Busto and coworkers [86], higher isomer selectivity was noted with the increase in aromatic content. This effect was also explained by the preferred adsorption of 1-methylnaphtalene to the strong acid sites, where cracking generally happens, resulting in an decrease on the cracking rate.

Transalkylation reactions can also occur on the catalyst acid sites, as studied by Almulla and coworker, who followed toluene reactions over Beta and Y zeolites with different Si/Al ratio to understand the effects of acid site strength on these transformations. Zeolite Y, which had lower Si/Al ratio, presented similar conversion as the beta zeolites, but stronger deactivation, which could be related to the formation of bigger coke precursors due to the presence of large super cages in zeolite Y. Selectivity towards xylenes was higher in the Beta zeolite, while Y zeolite (which has higher acidity) favored the production of trimethylbenzene and tetramethylbenze.[88], [89] These results show that the occurrence of secondary reactions of toluene, such as transklyations, depends on the acidity of the catalyst that is used.

Unlike cycloalkanes, aromatic impact on *n*-alkane hydrocracking seems to occur via two different reasons: preferential adsorption on acid sites or diffusion limitations caused by the size of the aromatic molecule. The specific molecule used in admixture also has an impact, as different size and chemical properties and can induce different effects over the same reaction. Shape selectivity induced by aromatic cofeed can lead to a shift in hydrocracking regime, since blocking the accessibility to some of the active sites can disturb the balance of the catalyst. However, it is worth noting that the ability to modify reaction rates and selectivity, by co-feeding certain aromatic compounds, can be used on reactor operations and catalyst design.

2.5 Thesis justification

The hydrocracking process is used to transform low value heavy oils into high value middle distillates, through isomerization and cracking reactions that occur over a bifunctional catalyst under hydrogen atmosphere. Currently, the state of the art provides enough data to understand the hydrocracking reaction mechanism over bifunctional catalyst as well as the influence of experimental conditions and metal-to-acid site ratio on the transition between ideal and non-ideal hydrocracking.

In industry, the hydrocracking feed is comprised of a mixture of alkanes, cycloalkanes and aromatic components. With such complex feed composition, it is expected to observe admixture impact on *n*-alkane hydrocracking. Several investigations studied the impacts of co-feed of alkanes and cycloalkanes on *n*-alkane conversion and isomer selectivity. It was found that heavier alkanes will generally have a negative impact in the conversion and isomer selectivity. Research regarding cycloalkane impact has shown that cyclic components will also reduce conversion and isomer selectivity due to preferential adsorption over the linear alkanes on catalyst active sites.

Unlike cycloalkanes, aromatic components can undergo two different reaction pathways, either following the classical bifunctional mechanism or reacting directly on acid sites, which could dictate different effects on *n*-alkane hydrocracking. Some investigations have shown negative impacts on *n*-alkane conversion due to preferential adsorption of aromatic molecules on acid sites or due to diffusion limitations induced by the size of aromatic components however, the full aromatic admixture effects on the hydrocracking mechanism and occurrence of ideal hydrocracking is still to be studied and understood, in order to optimize the reaction conditions (feed composition, catalyst, temperature, pressure, excess hydrogen) on industrial setting, achieving higher efficiency and better control over the product distribution.

The goals of the thesis are the experimental determination of aromatic component (toluene) impact on effective metal/acid site ratio for *n*-alkane (*n*-octane) hydrocracking over bifunctional catalyst (Pt/HUSY) at different operating conditions, while also assessing the influence of aromatic molecules on catalyst deactivation. The study of the impact hydrogen-to-hydrocarbon ratio will also be analyzed. This is achieved by following *n*-alkane conversion, isomer selectivity and catalyst activity under different conditions of pressure, temperature and space-times, over 0.3 wt% Pt/HUSY catalyst.

3. Experimental procedures

3.1 Catalyst Preparation

The Pt/HUSY catalyst was prepared using the incipient wetness impregnation method, as done in previous investigations [72][82]. Starting from the zeolite HUSY (CBV712 with molar SiO_2/Al_2O_3 ratio of 12, from Zeolyst), and tetraammineplatinum(II)-nitrate hexahydrate $[Pt(NH_3)_4](NO_3)_2 \cdot 6H_2O$ (from Sigma Aldrich (99,995% pure)) as platinum precursor. The platinum loading was 0.3 wt%. The precursor solution was prepared using the water saturation volume of the catalyst. The ratio between of water saturation mass and mass of dry zeolite was found to be 1.477. The precursor solution was then added drop-by-drop in different places of the crucible with zeolite and was homogenized by thorough stirring with a spatula in order to distribute the platinum as evenly as possible. After impregnation, the catalyst was left to mature overnight at room temperature after which it was dried in oven (produced by Memmert) at a temperature of 110 °C for 10 hours. Following the drying step, the catalyst crushed by mortar and then calcined in a calcination oven (model P330 by Nabertherm) where it was heated using the rate of 5 °C/min and kept at 150°C, 250°C and 350°C for one hour and at 500 °C for two hours. The temperature profile used for the calcination of the catalyst is shown in Figure 25.

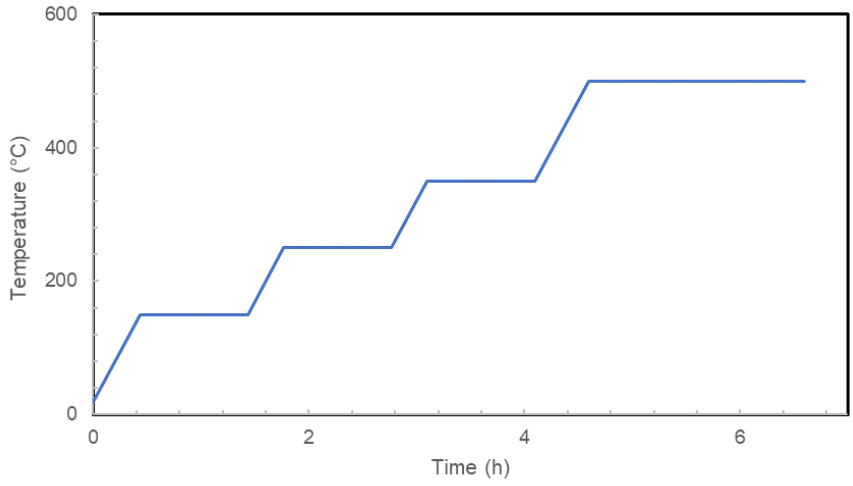

Figure 25: Temperature profile for the calcination of 0.3 wt% Pt/HUSY.

Previous investigations found that for catalyst particles with sizes comprised between 100 to 200 µm would ensure that no mass or heat transfer limitations would be present and secure the observation of intrinsic kinetics only. To achieve the desired range of particle size, the material was pelletized by applying 5 tons of pressure using a hydraulic press and was then sieved with a vibrating device (AS 200, by Retsch).

3.2 Catalyst Characterization

An insight in the physical and chemical properties is ensured by catalyst characterization. In this manner, various catalytic descriptors which control the kinetics of the reaction are defined (e.g., metal-acid site ratio, dispersion, etc.). As mentioned in section 2.3.1, metal-acid site ratio is a key controlling parameter of the hydrocracking regime and will be evaluated in this section. Furthermore, the platinum impregnation is evaluated. Different methods and techniques were used.

3.2.1 Nitrogen adsorption

Nitrogen adsorption-desorption was used to determine the pore volume and specific surface area of the catalyst on a TriStar II device, at 77 K. The t-plot method and the Brunauer, Emmett, Teller (BET) method, which assumes multilayer adsorption of the nitrogen molecules to the catalyst, were used to calculate the external surface area and pore volume.

3.2.2 Inductively Coupled Plasma Spectroscopy

Inductively Coupled Plasma Spectroscopy-Optical Emission Spectrometry (ICP-OES) was employed for the elemental analysis of the synthetized catalyst, with IRIS Intrepid II XSP from Thermo Scientific. The analyses were performed using method 3 (peroxide fusion), according to ISO 17025.

3.4.3 Hydrogen temperature-programmed reduction

Micromeritics Autochem II 2920 device was used to perform hydrogen temperature-programmed reduction (H_2-TPR). This method allows for the examination of the platinum reduction, which could be indirectly related to platinum dispersion as well. Using a thermal conductivity detector, the quantity of consumed hydrogen is known and with the platinum content it is possible to calculate the degree of platinum reduction. The temperature of the samples (0.3 g) was raised to 600 °C during one hour under a steady flow of 0.17 N mL/s of gas mixture with 5 vol% hydrogen in argon.

3.2.4 Hydrogen-oxygen titration

Hydrogen-oxygen titration was used to determine the platinum dispersion on the catalyst. The Autochem II 2920 device (Micromeritics) with thermal conductivity detector was used once more. The samples (0.2 − 0.3 g) were initially heated to 200 °C under hydrogen for 30 minutes and then at 450 °C for one hour. This was followed by cooling to 40 °C and consecutive pulses of hydrogen were injected every 3 minutes until adsorption was observed. In order to purge the surface of the catalyst, a flow of pure helium was employed for 45 minutes after which the pulse injection process was repeated, this time with oxygen until no further adsorption was observed. The samples were again purged, this time with argon for 45 minutes which was followed by a second cycle of reduction with hydrogen and oxidation with oxygen to guarantee repeatability.

Total number of accessible metal sites is calculated using the total volume of adsorbed hydrogen that on the metal sites, the molar gas volume, and the stoichiometry factor. The

dispersion was then obtained by the ratio of mass concentration of accessible metal sites over the total platinum concentration obtained with ICP-OES.

3.2.5 Transmission Electron Microscopy

Dark field transmission electron microscopy (STEM DF) allows for the investigation of the structure of the catalyst, as well as the platinum dispersion and particle sizes. This technique was done in a JEM-2200FS Cs corrected microscope device (JEOL) operated at 200 kV with Schottky type field emission gun (FEG) and EDX, with the catalyst sample being laid in a lacey carbon film with a copper grid support. The counts were done manually, using different images to achieve a better representation of the full surface of the catalyst.

3.2.6 Ammonia temperature-programmed desorption

With the objective to prove that the acidity of the zeolite does not change with platinum impregnation, ammonia temperature-programmed adsorption (NH_3-TPD) was used, using the AutoChem 2920 apparatus, produced by Micromeritics. The samples (0.1− 0.15 g) were firstly heated to 600 °C and the cooled down to 100 °C under constant flow of 1 mL/s of helium which was followed by a change in the gas composition to 4 vol% NH_3−He, while maintaining the flow rate of 1 mL/s to adsorb ammonia for one hour. After that, the sample was heated to 600 °C for 50 minutes, to assure all ammonia molecules would be desorbed, and the desorption rate was recorded by a thermal conductivity detector.

3.3 High-Throughput Kinetic Setup

The catalytic experiments were performed on the high throughput setup for mechanistic investigation designed by Zeton B.V (HTK-MI), [72][82][90] available within the Laboratory for Chemical Technology, at Ghent University. The setup consists of four blocks, each with two isothermal tubular reactors accommodated in a furnace, resulting in a total of eight reactors inside of the setup. Figure 26 shows the schematic overview of the high-throughput kinetic setup, where each reactor block can be divided into three sections: inlet section (liquid and gas feed), reactor system and analysis sections. [91]

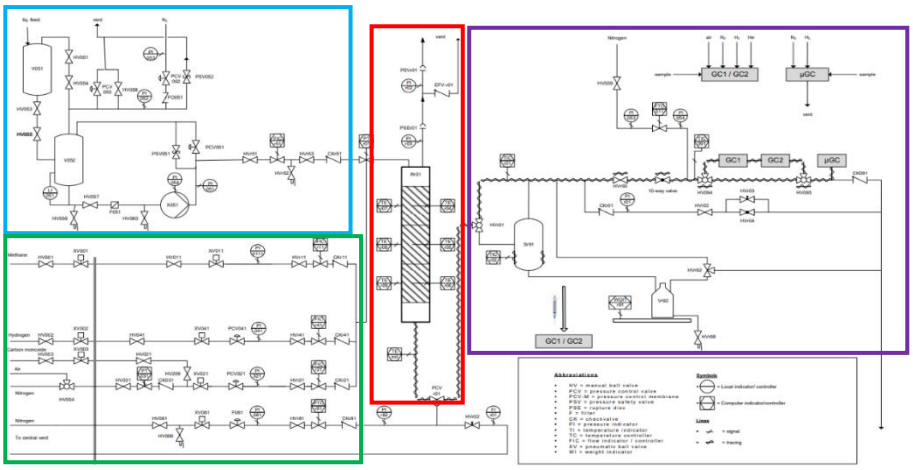

Figure 26: Schematic overview of the high-throughput kinetic setup. (blue: liquid feed section, green: gas feed section, red: reactor section, purple: analysis section). [91]

3.2.1 Inlet section

The feed section contains three gas and one liquid feed. The gas flow is controlled by means of mass flow controllers (Bronkhorst) calibrated for three different flow rates – 10 NL/h for methane, 100 NL/h for nitrogen and 1000 NL/h for hydrogen. The flows are set through the LabView software and control computer. Within this research all three gases were used: methane as the internal standard for analysis, nitrogen as a diluent and hydrogen as reactant and diluent. It is worth noting that methane can be obtained through dealkylation of toluene molecules however, giving that it requires the formation of a primary cation, which is not thermodynamically stable, the likelihood of these reactions to occur under the studied conditions is relatively low.

The liquid feed is supplied from the flask by HPLC pump (Knauer Azura P4.1s). The liquid feed is controlled by another mass flow controller (Bronkhorst) calibrated for *n*-octane flow rates between 10 and 50 g/h. Given the fact that liquid feed flow rates needed for performed experiments were lower than the calibrated range, the flow rate was controlled by HPLC pump. The liquid and gas feeds are mixed just before the reactor. The liquid feed was diluted with H_2 and N_2 to ensure a good distribution of the reactant throughout the catalyst bed. The dilution ratio was kept high to prevent possible condensation of reactants/products throughout the whole setup.

3.2.2 Reactor system

The reactor is situated inside the furnace and has an internal diameter of 11 mm and a length of 780 mm. It is made of ASI 316 cold worked steel, which allows for temperatures up to 649°C and pressure up to a maximum of 204 barg. [91]

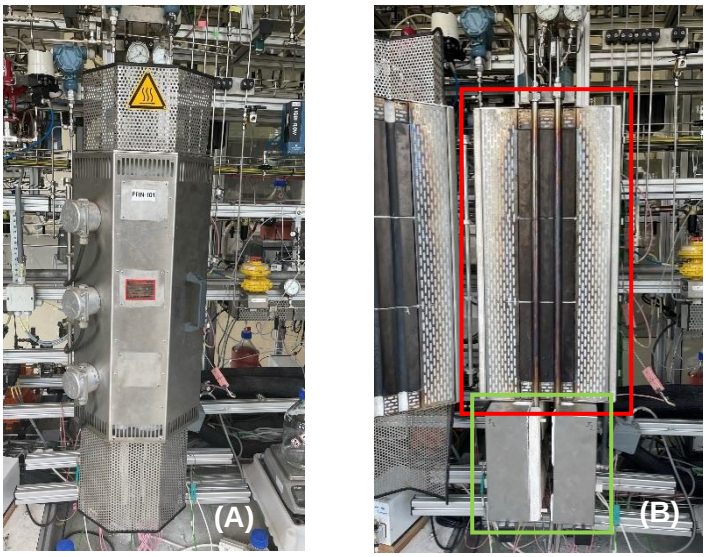

Figure 27: (A) Closed reactor block from the HTK setup closed (B) Open reactor block from the HTK setup (Red: Isothermal reactor with heating furnace; Green: Independent heating system – IR oven).

The temperature of each reactor is measured by two thermocouples with one of them being outside on the wall of the reactor, and the second one inside the tube in order to indicate temperature of the catalyst bed. Both thermocouples measure the temperature at three different locations along the reactor, which allows for the analysis of the temperature profile throughout the reactor. As highlighted in Figure 27 (B), immediately after the furnace there is an infrared oven (an independent heating block) set to 140°C to assure that no condensation of heavy hydrocarbons occurs in the reactor outlet. After this oven, all the remaining lines that connect the reactor to the analysis section are heat traced, such that temperature in the transfer line downstream the reactor is 200°C. This is done in order to have a reactor effluent in vapor phase.

The pressure inside the reactor is controlled using a back-pressure regulator (Equilibar H3P High Pressure). This regulator contains a membrane and is piloted by nitrogen flow. The pressure on membrane is set by a flow of nitrogen on LabView program for the setup control. In such a way membrane opens only when pressure exceeds a set point, allowing for a stable pressure within the reactor.

Catalyst bed is loaded prior to experimental campaign. In order to avoid mass and heat transfer limitations, inert α-Al_2O_3 particles are inserted. The reactor is initially filled up a layer of 1-2 cm height with inert particles of diameter of 5 mm. The layer of inert particles of diameter of 1-2 mm is added afterwards (height 7-10 cm). Above this layer is added the catalyst bed. The catalyst bed comprises catalysts particles of diameter between 100 and 200 µm and inert α-Al_2O_3 (diameter of 230 µm). The mass ratio of 1:3 (catalyst/inerts) ensures no mass and heat transfer limitation. Rest of the reactor is then filled up with inert particles with diameter between 1 and 2 mm. To ensure that the reacting gases reach the catalyst bed at the expected experimental temperature, the catalyst bed was placed in 8-12 cm above the end of the reactor. After the reactor, a filter was installed to prevent the escape of any particles to avoid damages to the reactor downstream, mainly to the membranes situated inside the back-pressure regulator.

During the experimental campaign, whenever catalyst deactivation was observed, the reactor was flushed with pure hydrogen between experiments to reactivate the catalyst, by hydrogenation of any aromatic compounds that could be located on the catalyst surface. Time on stream (TOS) tests were conducted to investigate catalyst stability at certain conditions, and it is counted as the time in which the reactants (*n*-octane or *n*-octane + toluene) flow through the reactor.

3.2.3 Analysis and Data Treatment section

After the back-pressure regulator, the reactor effluent is sent to a flash vessel where two phase flow is separated into gas and liquid flow. The gas flow is sent through a ten-way valve to an online gas chromatograph (GC) (850 Series II, Agilent Technologies) while the liquid flow of the reactor effluent is further sent to a storage tank. The chromatograph is equipped with a fire ionization detector (FID), which is one of the most sensitive gas chromatographic detectors for hydrocarbons, and a PONA column, where the products are retained based on their volatility resulting in a chromatogram with different peaks based on the number of carbon bonds broken by ionization.

In order to ensure correct identification of the peaks observed on the chromatograms, the GC was calibrated using a mixture of known linear alkanes and a second mixture of known cycloalkanes/aromatics. Toluene can either be transformed into methylcyclohexane (and isomers) or converted by acid catalyzed reactions into benzene and xylenes through transalkylation reactions. Since the residence times of these products is different than the ones expected for any of the products obtained from *n*-octane hydrocracking, no overlapping of peaks is expected, making it easier to correctly identify each peak that appear on the gas chromatogram. The relative area of each peak can be used to obtain the mass fraction of a certain component of the product stream, as shown in equation 1, where x_i is the mass fraction of product *i*, A_i corresponds to the relative area identified as the component *i* and CF_i is the correction factor for product *i*, which were obtained from Dietz. [92]

$$x_i = \frac{A_i CF_i}{\sum_{j=1}^{n} A_j CF_j} \quad (1)$$

Given that methane does not react and is not produced in *n*-octane hydrocracking, it can be used as the internal standard (IS). The mass flowrate of each component in the product stream is calculated by the set flowrate of internal standard, via the equation 2, where F represents the mass flow rate of component *i*.

$$F_i = \frac{F_{IS}}{x_{IS}} x_i \quad (2)$$

If the total weight of products and unreacted reactant equals the observed reactant mass flow rate within a 5% range, the mass balance is deemed as closed. Equation 3 shows how to obtain the conversion of component *i*, where F_i^0 is the inlet molar flow rate and F_i represents the outlet molar flow rate of the same component *i*.

$$X_i = \frac{F_i^0 - F_i}{F_i^0} \quad (3)$$

The selectivity towards a given product *i* or in relation to a given group of products (such as isomers or cracking products), is obtained using a carbon molar balance, as shown in equation 4, where FC_i represents the carbon molar flow rate of component *i* (or components belonging to a certain group) and FC_{PROD} corresponds to the carbon molar outflow of all the products originating from the reactant j. Isomer yield for a given product *i* is obtained by multiplying its selectivity by the conversion of reactant *j*, as demonstrated by equation 5.

$$S_i = \frac{FC_i}{FC_{PROD}} \quad (4)$$

$$Y_{i,j} = S_i X_j \quad (5)$$

Based on catalyst weight (W_{cat}) and the inlet molar flow rate of each reactant in the mixture (F_i^0), space times were obtained as shown by equation 6.

$$ST_i = \frac{W_{cat}}{F_i^0} \quad (6)$$

4. Results

In this section, the obtained results throughout the investigation will be shown. Section 4.1 presents the results from the catalyst characterization and their comparison with literature, allowing for a better understanding of the physical and chemical properties of the catalyst.

Section 4.2 focuses on the results obtained from the catalytic tests and their interpretation. The tests were done with a mixed feed comprised of alkane (*n*-octane) and aromatic (toluene) components, over different process conditions over Pt/HUSY catalyst.

4.1 Catalyst Characterization

4.1.1 Nitrogen adsorption

The specific surface area of the synthetized catalyst was determined through nitrogen adsorption. The nitrogen adsorption-desorption isotherm obtained is shown in Figure 28. The isotherm resembles a combination between type I and type IV, where the adsorption proceeds via multilayer adsorption followed by capillary condensation on the mesopores, identified by the hysteresis loop observed on Figure 28. This isotherm is characteristic for the presence of both micro and mesopores. [93]–[95]

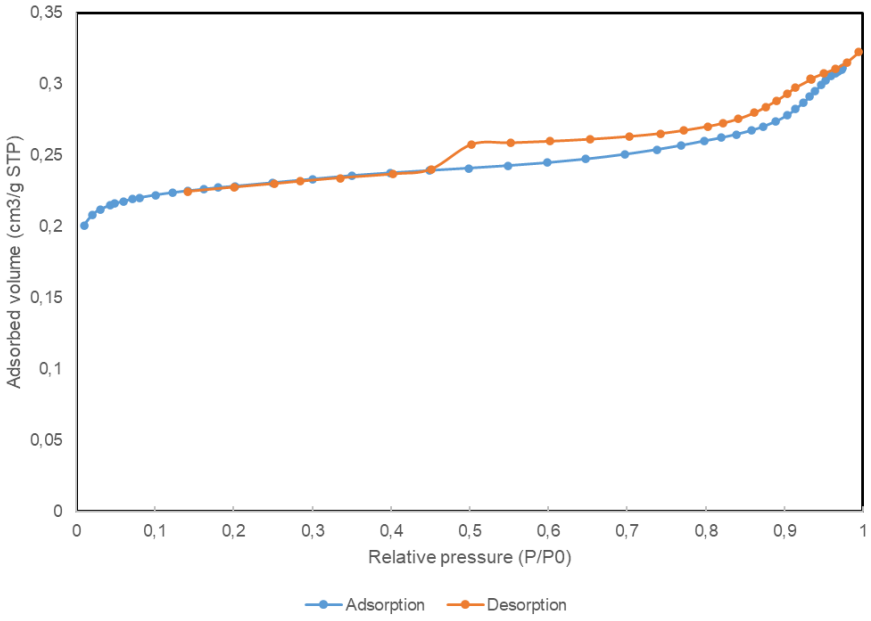

Figure 28: Nitrogen adsorption-desorption isotherm for 0.3 wt% Pt/HUSY catalyst.

The elementary reactions of isomerization and cracking occur in the Brønsted acid sites, which are located inside the micropore structure of the zeolite. Due to this, it is important to ensure that the micropore volume and surface area are consistent with what was previously reported since decreasing the available space for reaction can negatively impact catalyst activity.

The results obtained through the t-plot method are listed in Table 7 and are compared with previous research done with catalyst with the same Pt loading [82]. As can be observed from

Table 7, surface area and micropore area is constant between the two catalysts. The same can be said regarding the micropore volume.

Table 7: Results obtained from N_2 adsorption of synthetized catalyst and comparison with previous research.

	Synthetized catalyst	Literature [82]
Micropore volume (cm^3/g)	0.293	0.295
Micropore area (m^2/g)	602	570
External surface area (m^2/g)	138	149

4.1.2 Inductively Coupled Plasma Spectroscopy

The platinum content of the synthesized catalyst was confirmed by Inductively Coupled Plasma Spectroscopy. The obtained content was very close to the one that was expected, with a deviation of approximately 4%, which can be considered as negligible. This technique allowed for the calculation of the theoretical concentration of Brønsted acid sites using SiO_2/Al_2O_3 ratio obtained with ICP-OES and the fractions of Al(IV) and extraframework Al atoms for HUSY found in literature [96]–[98], as done in previous studies [72][82]. The Brønsted acid sites concentration is equal to the concentration of Al(IV) atoms, which is calculated based on the fraction of Al(IV) retrieved from literature. The concentration of strong acid sites is obtained with the mass of zeolite and then, together with platinum content, is then used to determine the metal/acid sites ratio. The results obtained are shown in Table 8.

Table 8: Elemental composition of the synthetized catalyst obtained by ICP-OES.

	Pt (wt%)	Si/Al	H^+ concentration (mmol/g catalyst)
0.3 wt% Pt/HUSY	0.311	7.02	1.93

4.1.3 Hydrogen temperature-programmed reduction

Hydrogen temperature-programmed reduction was used to examine the degree of platinum reduction. In this technique, a flow of hydrogen passes over the surface of the catalyst with gradually increasing thermal conditions, reducing the metal.

The reduction curve obtained can be found on Figure 29 and the area below the reduction curve reflects the amount of hydrogen consumed. Two peaks can be identified, at temperatures of 425°C and 600°C, which correspond to the two most common platinum oxidation states: +4 and +2. Pt(IV) is easier to reduce, which means that lower temperatures are required thus it corresponds to the first observed peak.

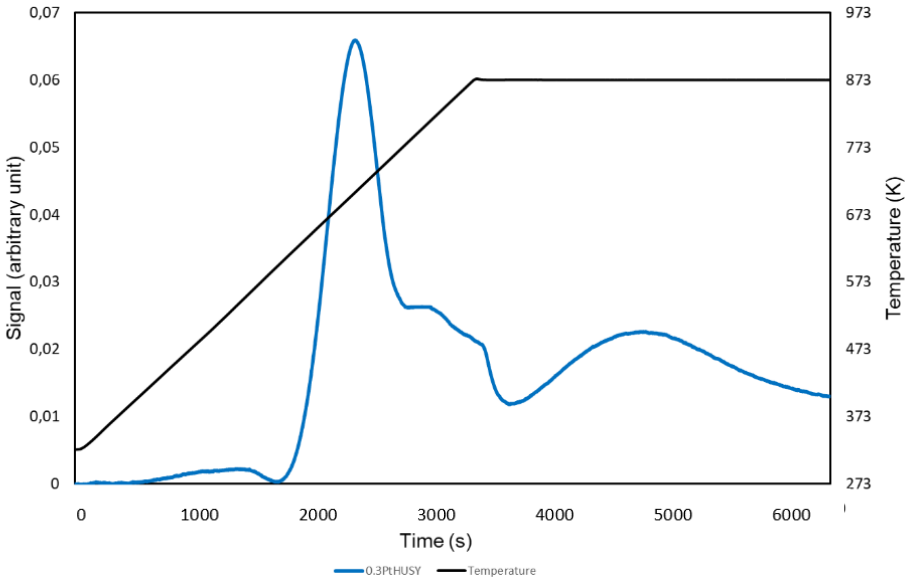

Figure 29: Hydrogen temperature programmed reduction of studied 0.3 wt% Pt/HUSY catalyst.

Table 9: Results obtained from hydrogen temperature-programmed adsorption of 0.3 wt% Pt/HUSY catalyst.

	Quantity of consumed H_2 (cm^3 STP/g)	Reduction degree (%)	n_{Pt}/n_{H+} x 10^3 (mol/mol)
0.3 wt% Pt/HUSY	0.250	36.5	5.76

The achieved reduction degree for the 0.3 wt% Pt/HUSY synthesized catalyst was 36.5% which is similar to the one obtained in previous studies (36%) [82]. Using the acid site concentration obtained with NH_3-TPD and the platinum content from ICP-OES, the theoretical metal-to-acid ratio was calculated, and reduction degree was applied.

4.1.4 Hydrogen-oxygen titration

Hydrogen-oxygen titration technique was used to obtain platinum dispersion and average particle size on the catalyst. The results obtained are organized in Table 10. The metal dispersion obtained through hydrogen-oxygen titration was found to be low and almost one third of the reduction degree of platinum, obtained by H_2-TPR (36.5%). The particle size obtained with H_2-O_2 titration is higher than the average particle size observed by TEM (1.09 nm), since the dispersion value obtained from H_2-O_2 titration was found to be relatively low. Given the results obtained from TEM and H_2-TPR, the results from H_2-O_2 titration do not seem reliable.

Table 10: Results obtained from hydrogen-oxygen titration of 0.3 wt% Pt/HUSY catalyst.

Dispersion (%)	**13.04**
Particle size (nm)	8.69

4.1.5 Transmission Electron Microscopy

The distribution of platinum particle sizes over the surface of the catalyst was assessed using transmission electron microscopy. Figure 30 shows a representative image of 0.3 wt% Pt/HUSY catalyst and other images obtained through transmission electron microscopy are present in the Annex A. The manual counts obtained with this method are shown in Figure 31.

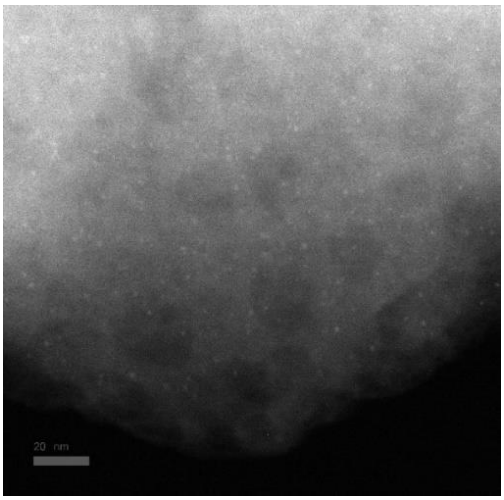

Figure 30: TEM image of 0.3 wt% Pt/HUSY catalyst.

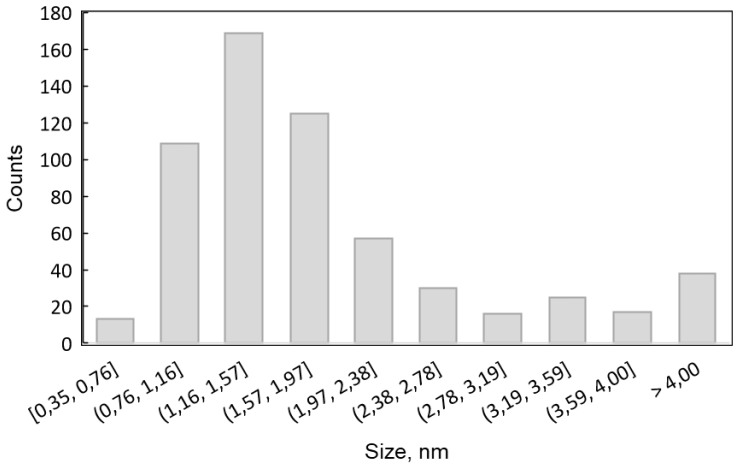

Figure 31: Platinum particle sizes distribution over 0.3 wt% Pt/HUSY catalyst, obtained through TEM.

Observing Table 11, where the results obtained are summarized, it is possible to acknowledge that the average diameter is higher than what was obtained in previous investigation for catalyst with the same platinum content (1.4 nm) [82]. Higher average particle size can indicate low platinum dispersion, since previous research has shown that smaller particles lead to dispersion values of 82% [82], for catalyst with the same metal loading. Figure 30 allows for a similar conclusion given the presence of a few large agglomerates of platinum on the surface of the catalyst.

Table 11: Average particle size, standard deviation and minimum/maximum sizes obtained by TEM.

	Average (nm)	Standard Deviation (nm)	Minimum (nm)	Maximum (nm)
0.3 wt% Pt/HUSY	1.9	1.0	0.35	5.8

4.1.6 Ammonia temperature-programmed desorption

In Figure 32 is shown the comparison of ammonia temperature-programmed desorption (NH_3-TPD) for pure HUSY (CBV712) zeolite and 0.3 wt% Pt/HUSY. From literature, it is known that ammonia temperature-programmed desorption does not allow for the identification of the nature of acid sites (Brønsted and Lewis acid sites) [99]. However, two peaks can be observed in

Figure 32. Since Brønsted acid sites are stronger, more energy is needed for ammonia desorption from these acid sites, which means that the peak corresponding to these active sites should be observed at higher temperatures. The area under the curve of the catalyst corresponds to the volume of desorbed ammonia. Concentration of all acid sites are calculated based on this volume. The results obtained and the values from literature [82] are shown in Table 12. Given that the curves obtained for the HUSY zeolite and the catalyst do not differ much from each other (especially for strong acid sites), it can be concluded that the acidity of the catalyst is not changed by platinum loading. In comparison with values obtained from previous investigations [82], the obtained values of acidity and quantity of desorbed NH_3 were found to be very similar to the ones reported in literature.

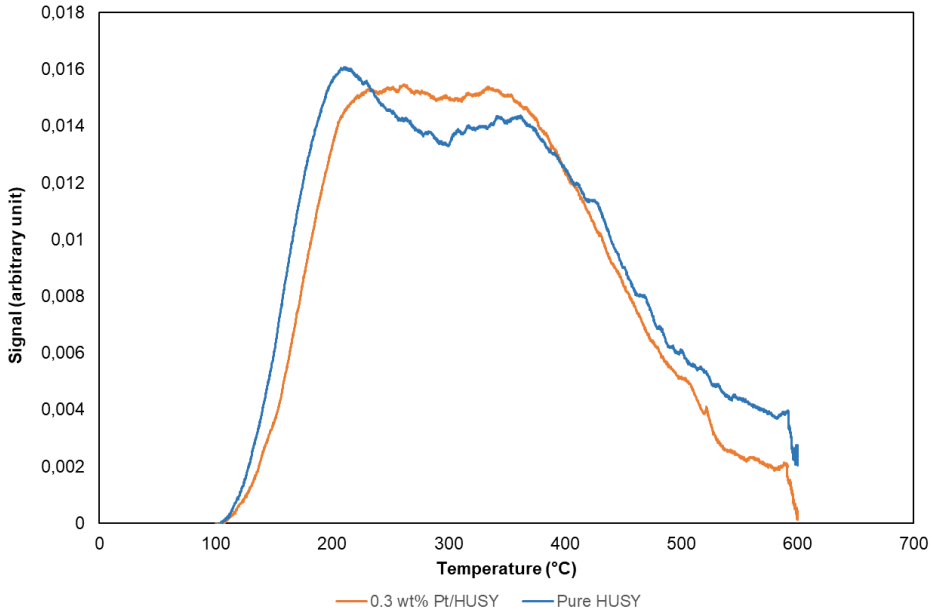

Figure 32: Ammonia temperature programmed desorption of pure HUSY zeolite and synthetized 0.3 wt% Pt/HUSY catalyst.

Table 12: Results obtained from NH_3-TPD of synthetized catalyst and comparison with pure zeolite.

	Quantity of desorbed NH_3 (cm^3 STP /g)	Acidity (mmol/g)
Pure HUSY	25.47	1.14
Pure HUSY – literature [100]	----	1.04
0.3 wt% Pt/HUSY	22.55	1.01
0.3 wt% Pt/HUSY – literature [82]	22.83	1.02

The theoretical concentration of Brønsted acid sites (1.93 mmol/g) is higher than the one obtained through NH_3-TPD. The latter represents the correct metal-to-acid sites ratio since it

corresponds to the accessible platinum sites. This value was used to calculate the metal-to-acid site ratio (5.76 x10^3 mol/mol) with said of ICP analyses and metal reduction degree.

Earlier investigation by Korica et al. [63] showed that a metal-to-acid site ratio of 1.56 (x10^3 mol/mol) is enough to ensure ideal hydrocracking of *n*-octane for Pt/HUSY at applied operating conditions [72]. With this in mind, and despite the relatively low degree of reduction, since the calculated metal-to-acid site ratio with dispersion is higher than the ratio obtained in previous studies, the synthetized catalyst should be able to also ensure the ideal hydrocracking of *n*-octane over similar experimental conditions. It is also worth noting that the synthetized catalyst has similar metal-to-acid site ratio in comparison with a catalyst with the same metal loading from previous research (7.1 x10^3 mol/mol) [82].

4.1.7 Conclusions

The characterization results were summarized in Table 13 and show the physico-chemical properties of the synthetized 0.3 wt% Pt/HUSY. Based on the results, the addition of platinum particles did not impact the acidity of the zeolite and from the ICP analysis, it was concluded that the elemental composition and Si/Al were similar to what was expected. Porosity and surface area were also close to what has been previously reported. Larger particles were observed with TEM, when compared with previous results [82], which could also be seen with the relatively low reduction degree obtained by H_2-TPR and could be possibly be explained by improper calcination conditions.

The metal dispersion of the catalyst and average particle size, obtained with H_2-O_2 titration, were found to be relatively poor, leading to the conclusion that these results were not reliable. The theoretical concentration of Brønsted acid sites was calculated using the values of Si/Al ratio obtained through ICP and was used to determine the metal-to-acid sites ratio of the catalyst considering the metal reduction.

Table 13: Summary of the obtained results from catalyst characterization.

		0.3 wt% Pt/HUSY
Pt loading (wt%) - ICP		0.311
Pt reduction degree (wt%) – H_2 TPR		36.5
Pt dispersion (%) – H_2-O_2 titration		13.0
n_{Pt}/n_{H+} x10^3 (mol/mol)		5.76
Acidity (mmol/g) – NH_3 TPD		1.01
Specific surface area (m^2/g) - N_2 adsorption t-plot		602
Average particle size (nm)	TEM	1.09

4.2 Catalytic Kinetic studies

4.2.1 Definition of the experimental space

For this experimental campaign, the selected model compounds for alkane and aromatic were *n*-octane and toluene, respectively. These components are representative for the paraffins and aromatic molecules present in oil fractions that are generally subject to hydrocracking [101]. *n*-octane reaction network is extensive enough to efficiently observe transitions between ideal and non-ideal hydrocracking. Alkanes with higher carbon number result in a larger number of different products, which could be difficult to correctly identify during the analysis step [70]. On the other side, shorter alkanes could prove to be ineffective for the detection of ideal hydrocracking, since the less extensive reaction network could hinder the equilibrium between mono-, di- and tribranched isomers observed in ideal hydrocracking, mentioned in section 2.2.1. Given that toluene can react either directly on acid sites or be hydrogenated on metal sites, the reaction network of this component allows for the observation of both reaction pathways, and its influence on *n*-octane conversion/isomer selectivity can be analysed.

In terms of GC detection, the toluene hydrocracking products do not overlap with the isomerization/cracking products of the hydroconversion of *n*-octane, as no ring-opening reactions of toluene occurs, thus making it possible to distinguish the products from toluene and *n*-octane reactions. Generally, aromatic molecules tend to adsorb preferentially over linear alkanes with the same carbon number [64] however, from Table 14, it is possible to observe that the physisorption enthalpies of *n*-octane and toluene over USY zeolite with different Si/Al ratios are comparable [51][68][102][103] and thus it can be considered their physisorption tendencies as similar, despite having different carbon number. The two components also have other similar properties, as indicated in Table 14, which ensures that any observed impact is solely due to the chemical properties of toluene.

Table 14: General properties and physisorption enthalpies of n-octane and toluene. [68][102]–[105]

	***n*-octane**	**toluene**
Carbon number	8	7
Molar mass (g/mol)	114.23	92.14
Boiling Point (°C)	111	125
Physisorption enthalpy (kJ/mol)	59.9 (Si/Al=2.7) [51]	54.3 (Si/Al=11) [102]
	56.5 (Si/Al=30) [68]	58.4 (Si/Al=30) [68]
	49.9 (Si/Al=41) [51]	69.8 (Si/Al=40) [102]

The operating conditions were selected to ensure a broad range of *n*-octane conversion (10% - 55%) in order to have minimal experimental error and reliable comparison between kinetic measurements. The experiments were conducted at two total pressures (10 and 20 bar) which allows identification of ideal hydrocracking regime. The admixture effect of toluene was experimentally assessed by using 4:1 n/n mixture of *n*-octane and toluene as it can be reasonably

assumed that this content is highly representative for the realistic aromatic content in hydrocarbon feed. As seen in Section 2.2.3, toluene can follow two different reaction pathways, with one of them being the classic hydrocracking mechanism over bifunctional catalyst, being hydrogenated on the metal sides of the catalyst followed by isomerization/cracking reaction on acid sites, and the other being the direct reaction of toluene carbenium ions on acid sites, through transalkylation and disproportionation reactions. The impact of hydrogen-to-hydrocarbon molar ratio was analyzed in this experimental campaign since lower hydrogen partial pressure could reduce the rate of the hydrogenation reaction leading to toluene reacting directly on the acid sites without prior hydrogenation, resulting in the formation of compounds like xylenes and benzene. The partial pressure of *n*-octane and toluene remained constant during all the experiments with lower hydrogen-to-hydrocarbon ratio by addition of nitrogen as inert diluent. 0.1wt% Pt/HUSY catalyst ensures ideal hydrocracking of pure *n*-octane at similar operating conditions [72]. however, with the introduction of toluene to the feed, a catalyst with higher platinum loading was used (0.3 wt% Pt/HUSY). Experimental conditions applied in this experimental campaign are summarized in Table 15.

Table 15: Experimental conditions used in the experimental campaign.

Catalyst	Feed composition (mol/mol)			Temperature (°C)	Pressure (bar)	Space time (kg s/mol)	H_2/HC ratio (mol/mol)	N_2/H_2 ratio (mol/mol)	Partial Pressure (bar)	
	n-octane		toluene						*n*-octane	toluene
0.3 wt% Pt/HUSY	1	:	0	270 - 290	10 - 20	300 - 615	100 - 200	(no N_2 was used)	0.10	0
	4	:	1	270 - 290	10 - 20	300 - 615	80 - 170	(no N_2 was used)	0.10	0.025
	4	:	1	270 - 290	10 - 20	300 - 615	6.5	11.5 – 24	0.10	0.025

4.2.2 Pure *n*-octane feed

The first set of experiments was done with a pure *n*-octane feed to prove that the catalyst was well balanced at applied conditions. In this way a reliable comparison with experiments with toluene admixture is assured. The results obtained for the conversion of *n*-octane over 0.3 wt% Pt/HUSY catalyst for different conditions were obtained through the average of different GC analysis over several hours of time on stream, corresponding to steady-state, and are shown in Figure 33.

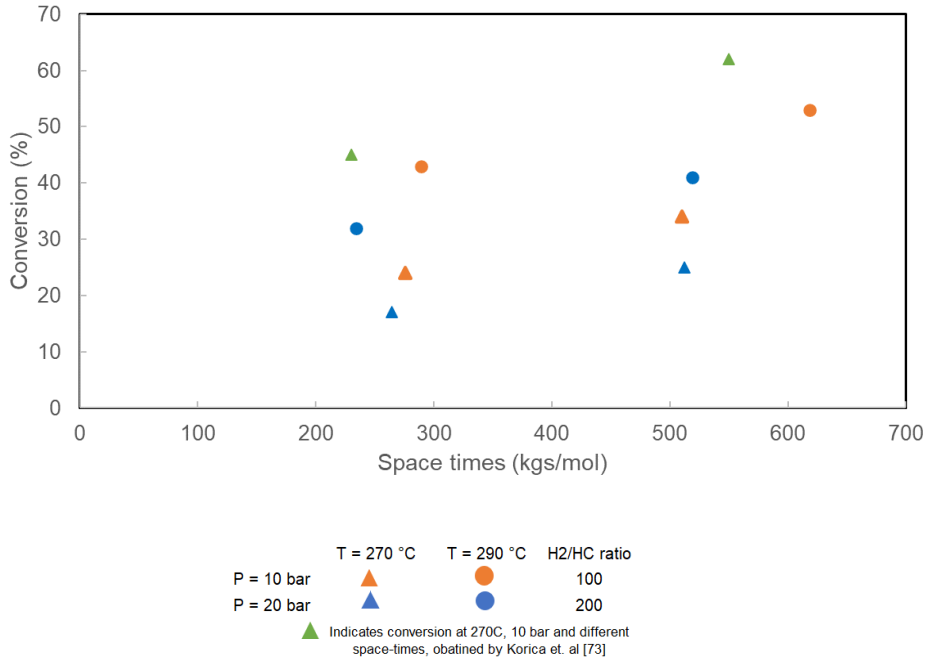

Figure 33: n-octane conversion, when fed pure at different temperatures and pressures, high hydrogen-to-hydrocarbon ratio, as a function of space time calculated based on n-octane flow over 0.3 wt% Pt/HUSY. Green triangles indicate results obtained in previous investigations by Korica et al. [82] used for comparison.

Figure 33 shows *n*-octane conversion obtained under different experimental conditions as a function of space time and it is possible to identify the trends mentioned in section 2.3.2 which indicate ideal hydrocracking occurrence - such as a decrease of *n*-octane conversion for higher total pressure. Based on the results from the previous work by Korica et al [82] (see Figure 33), higher conversions are expected at applied conditions. It seems that that complete mass of catalyst is not utilized, probably due to channeling inside the catalyst bed or incorrect activation, which could be related to poor catalyst loading on the reactor. The difference in conversion could also be explained by the presence of relatively large platinum agglomerates (see section 4.1.5), which indicates that not all metal particles are accessible for reaction. Despite of this, the catalyst can still be considered as well-balanced as conversion decreases with total pressure and isomer yield is comparable with previous investigations.

4.2.3 Experiments with the mixture of *n*-octane and toluene (4:1 n/n) and high H_2/HC ratio

The experiments with mixed feed of 4:1 n/n *n*-octane/toluene were carried out to assess the impact of toluene co-feed on the hydrocracking of *n*-octane. The experiments were done by keeping partial pressure of *n*-octane constant as in the experiments with pure *n*-octane. In order to do so, hydrogen-to-hydrocarbon ratio was slightly adjusted. However, this change of H_2/HC ratio was very minor so that it does not influence the occurrence of ideal hydrocracking.

In order to evaluate the stability of the catalyst, time on stream (TOS) tests were done in parallel at different temperatures and space-times. Figure 34 (270 °C, 10 bar, 1g/h) and Figure 35 (290 °C, 10 bar, 2g/h) show that the catalyst remained active after the incorporation of toluene

in the feed, given that the conversions remained approximately constant for at least four hours of time on stream.

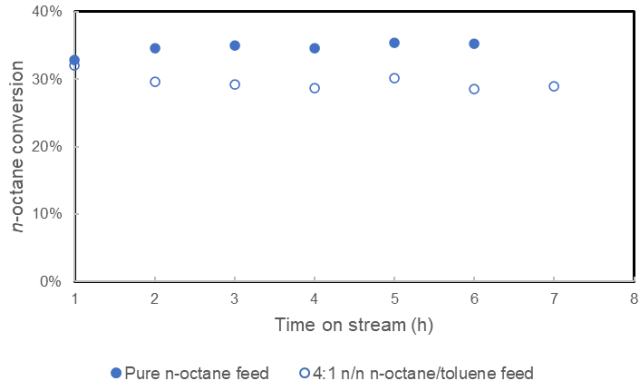

Figure 34: n-octane conversion, when fed pure or in a 4:1 n/n mixture with toluene and high hydrogen-to-hydrocarbon ratio, at 270 °C, 10 bar, 1 g/h, as function of time on stream.

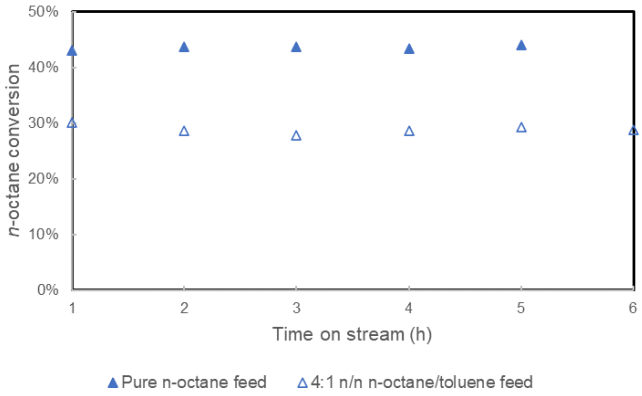

Figure 35: n-octane conversion, when fed pure or in a 4:1 n/n mixture with toluene and high hydrogen-to-hydrocarbon ratio, at 290 °C, 10 bar, 1g/h as function of time on stream.

The *n*-octane conversion obtained at different conditions of temperature, pressure and space time (previously introduced in Table 15) when the feed consists of pure *n*-alkane (full symbols) and when the feed is a 4:1 n/n mixture of *n*-octane and toluene (empty symbols) is shown in Figure 36. No significant change in conversion for most of the experimental points was observed. However, there is one experimental point (T=290 °C, P=10 bar, ST=288 Kgs/mol) that shows a considerable decrease in conversion when *n*-octane is fed pure compared to when it is fed in combination with toluene. Given the fact that this behavior is only noted for this single point, it can be considered as an outlier. No shift from ideal to nonideal hydrocracking is induced. This claim is validated by Figure 37, where the *n*-octane isomer yield is maximal regardless of the feed composition.

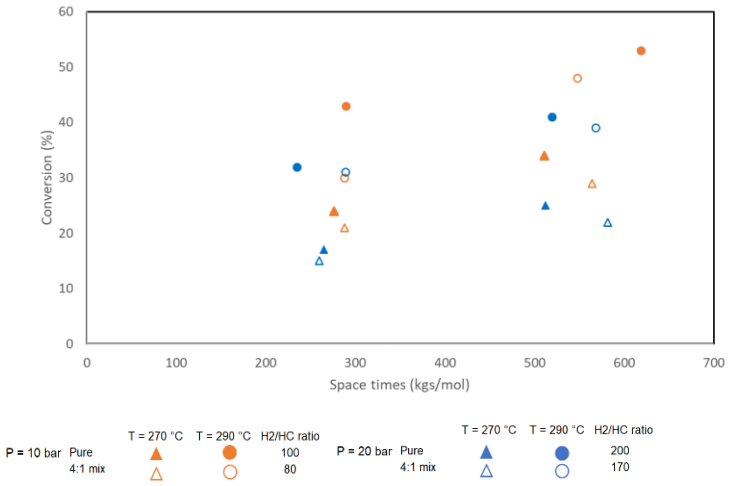

Figure 36: n-octane conversion, when fed pure (full symbols) or in a 4:1 n/n mixture with toluene and high hydrogen-to-hydrocarbon ratio, at different temperatures and pressures, as a function of space time calculated based on n-octane flow over 0.3 wt% Pt/HUSY.

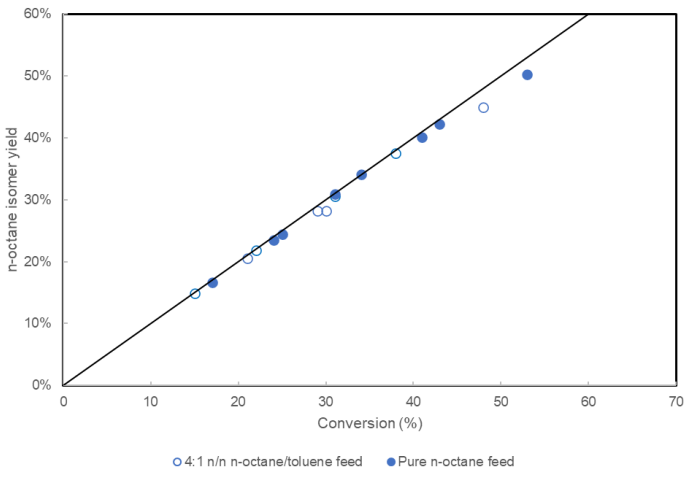

Figure 37: n-octane isomer yield, when fed pure (full symbols) or in a 4:1 n/n mixture with toluene and high hydrogen-to-hydrocarbon ratio, as a function of n-octane conversion.

4.2.4 Experiments with the mixture of *n*-octane and toluene (4:1 n/n) and low H_2/HC ratio

As mentioned in chapter 2.2.3, over bifunctional catalyst toluene can undergo different reactions thus yielding different products and possibly have distinct effects on the hydrocracking of *n*-octane. The concentration of H_2 can impact the reaction mechanism of the aromatic molecule since higher hydrogen concentration promotes the dehydrogenation of aromatics on metal sites so, in order to study the impact of excess hydrogen, the hydrogen-to-hydrocarbon ratio was lowered to 6.5, as presented in Table 15, with nitrogen being added as inert gas to keep the partial pressures of *n*-octane and toluene constant over all the experiments. Figure 38 shows conversion of *n*-octane as function of time-on-stream obtained for each set of conditions with pure *n*-octane feed and with the mixed feed of *n*-octane/toluene with a hydrogen-to-hydrocarbon ratio of 6.5.

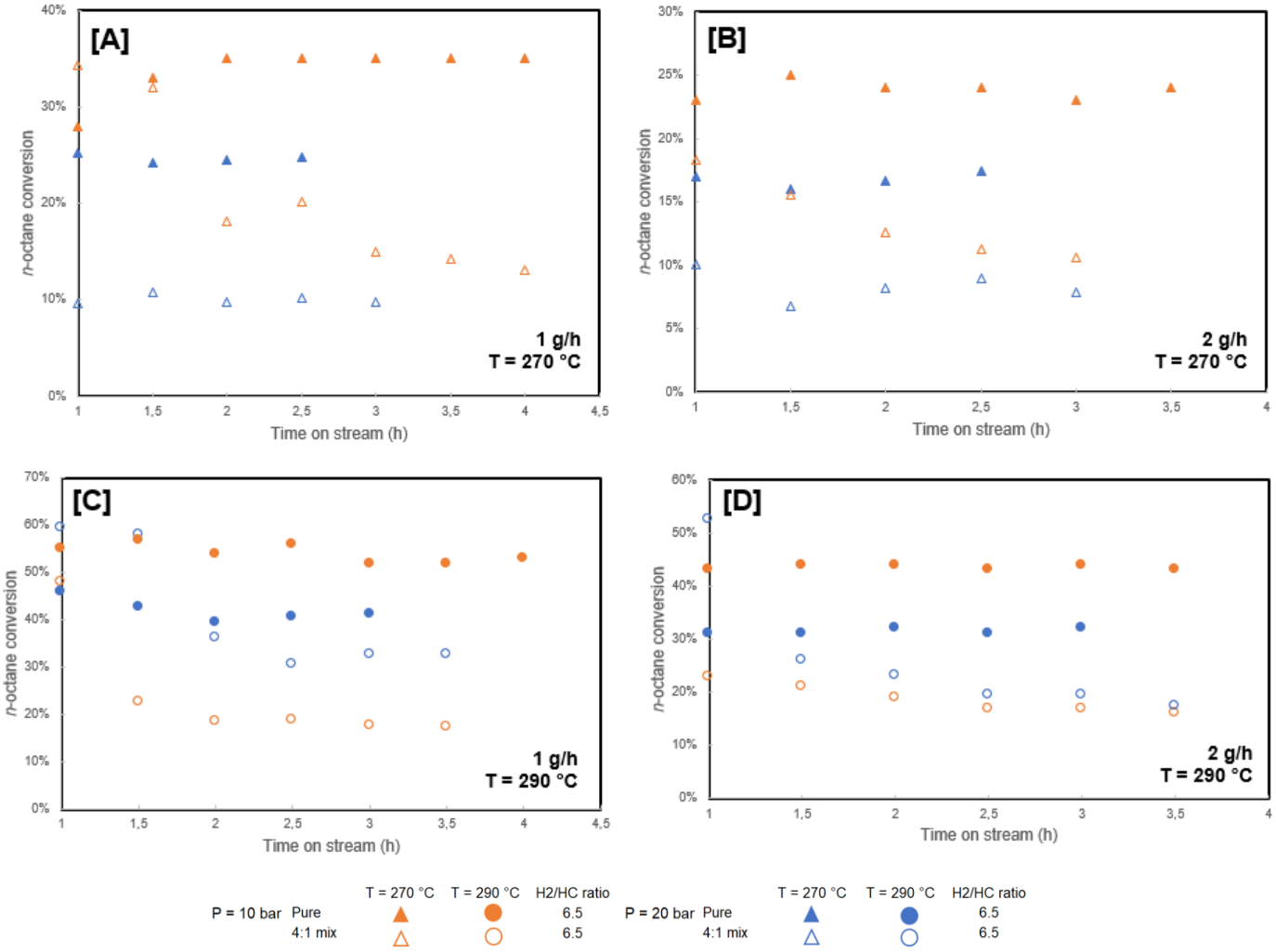

Figure 38: n-octane conversion, when fed pure (full symbols) or in a 4:1 n/n mixture with toluene and hydrogen-to-hydrocarbon ratio of 6.5, at different temperatures and pressures, as function of time on stream.

In general, at the most of experimental conditions, catalyst deactivation was observed. This effect was more pronounced at lower pressure as can be observed on Figure 38-(C) and Figure 38-(D). In these figures it is recognized that the conversion decrease at 10 bar is 30% (290 °C, 1 g/h) and 25% (290 °C, 2 g/h) while the drop in *n*-octane conversion at 20 bar is only around

10% in both cases. The deactivation also appears to be more pronounced when higher space times (lower liquid flow) is employed. It is also possible to detect a shift to non-ideal hydrocracking when the temperature is 290 °C, given that the conversions obtained for pressure of 20 bar are higher than the *n*-octane conversions reached when the pressure is lower. The intensity of catalyst deactivation also seems to be related to total pressure. It is observed that higher pressure leads to less deactivation of the catalyst, since it reduces the amount of bimolecular reactions of toluene on acid sites which lead to coke formation. Increases in pressure lead to increases in nitrogen (inert gas) partial pressure, as the partial pressures of toluene and *n*-octane are kept constant throughout all experiments. This results in less frequent molecular collisions between toluene molecules and thus, less reactions that result in coke precursors.

The *n*-octane isomer yield was also studied when the hydrogen-to-hydrocarbon was lowered to 6.5 and is present on the Figure 39.

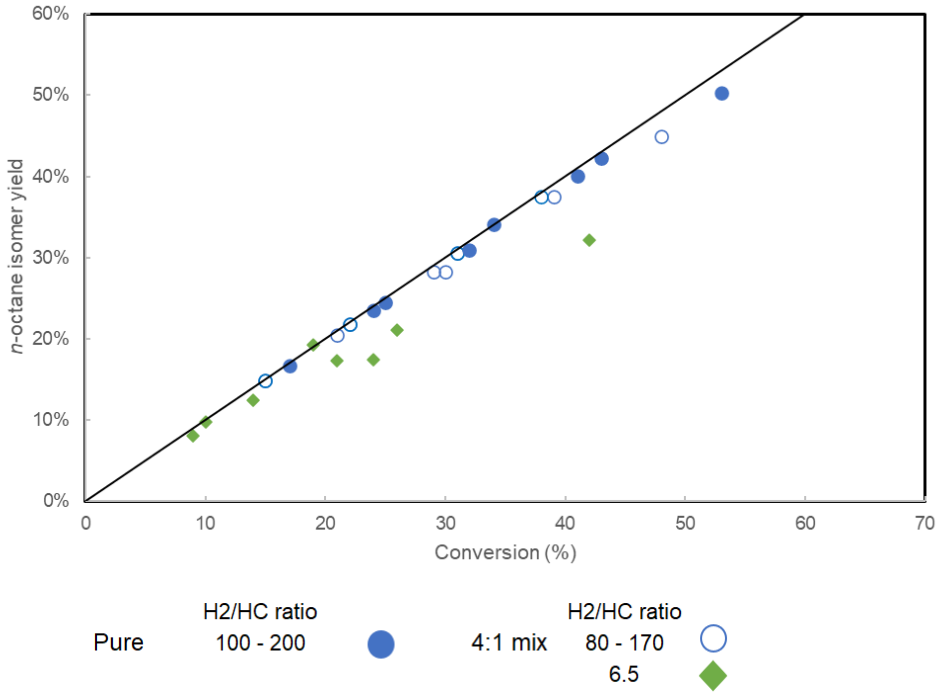

Figure 39: n-octane isomer yield, when fed pure (full symbols); in a 4:1 n/n mixture with toluene and high hydrogen-to-hydrocarbon ratio (blue circles) or in a 4:1 n/n mixture with toluene and hydrogen-to-hydrocarbon ratio of 6.5 (green diamonds), as a function of n-octane conversion.

The characteristic isomer yield of ideal hydrocracking is respected at lower conversions (10% - 20%) however, some deviation from this ideal behavior is observed at higher *n*-octane conversions (24% - 42%) which indicates a shift to non-ideal behavior. These experimental points were all taken at 290 °C, which verifies that at this temperature the ideal hydrocracking is no longer occurring as also pointed in Figure 38-(C) and Figure 38-(D). As consequence of this transition in hydrocracking regime, selectivity towards *n*-octane cracking products increased at higher temperature.

In order to fully understand the effect of toluene on *n*-octane hydrocracking, the conversion and product selectivity of the aromatic molecule were also analyzed. As mentioned in before, toluene can either be hydrogenated on metal sites resulting in methylcyclohexane which follows the classical bifunctional mechanism, or it can directly react on the acid sites through disproportionation or transalkylation reactions. Consequently, it is possible to draw some conclusions regarding the reaction mechanism of toluene and its impact on the hydrocracking of *n*-octane.

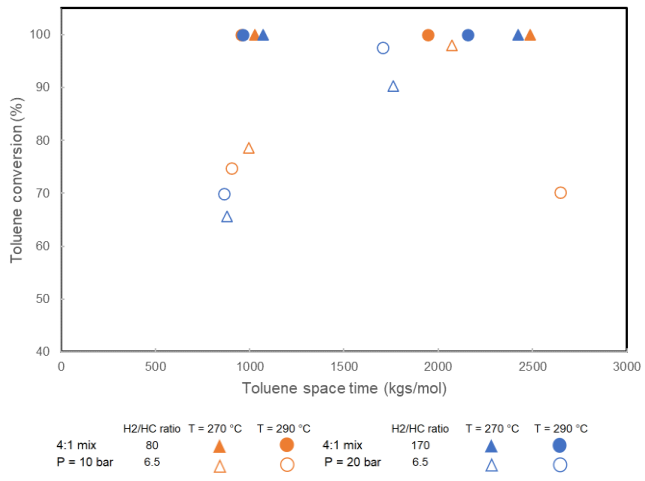

Figure 40: Toluene conversion, when fed with high hydrogen-to-hydrocarbon ratio (full symbols) or hydrogen-to-hydrocarbon ratio of 6.5, at different temperatures and pressures, as function of space time calculated based on toluene flow over 0.3 wt% Pt/HUSY.

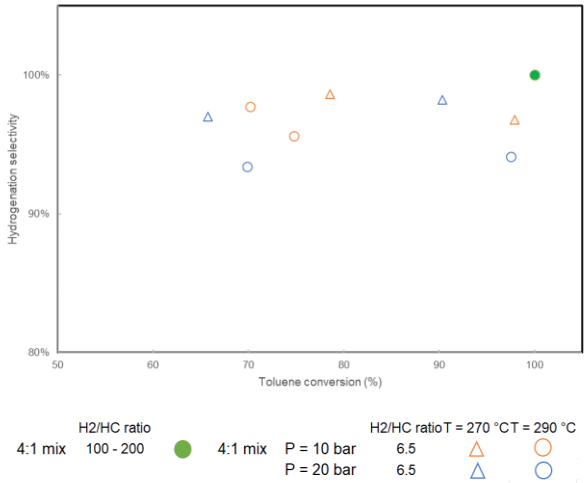

Figure 41: Toluene selectivity to hydrogenation products, when fed with high hydrogen-to-hydrocarbon ratio (green) or hydrogen-to-hydrocarbon ratio of 6.5, at different temperatures and pressures, as function of toluene conversion.

From Figure 40 it is possible to observe that for the reactions that are not in thermodynamic equilibrium, lower space times result in decreased toluene conversion. However, at temperature of 290 °C higher pressure leads to an increase in toluene conversion.

4.2.5 Discussion and conclusions

As mentioned in section 2.2.3, aromatic molecules, unlike saturated hydrocarbons, can follow two different pathways over a bifunctional catalyst. Toluene can undergo one of the two reaction pathways shown in Figure 42, where A represents the classic bifunctional mechanism, where the aromatic is hydrogenated on metal sites and B shows the reactions that occur directly on acid sites, through transalkylation and disproportionation reactions yielding benzene and xylenes. Understanding the reaction network of toluene is crucial to interpret the experimental results of this campaign.

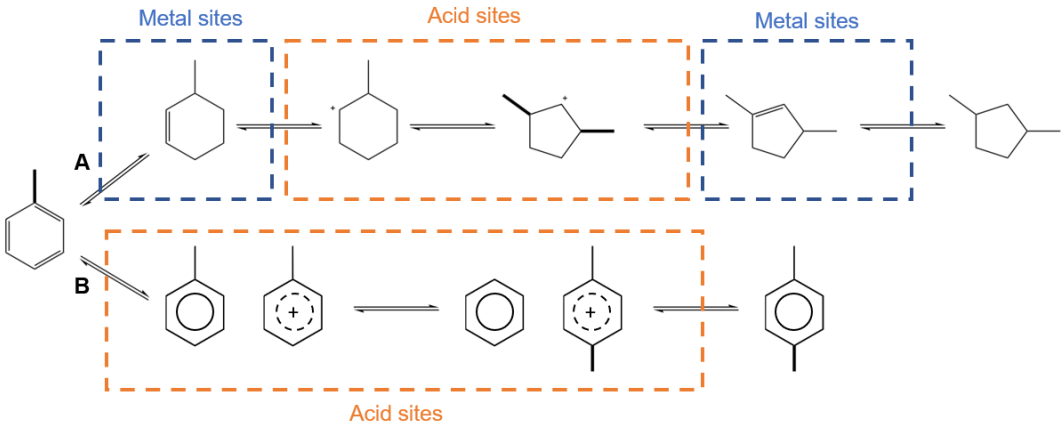

Figure 42: Possible toluene reaction schemes under low hydrogen-to-hydrocarbon ratio conditions.

When high hydrogen-to-hydrocarbon ratio was used, no deactivation or decrease in n-octane conversion was observed. With high excess hydrogen, toluene was completely hydrogenated to methylcyclohexane, which followed further bifunctional mechanism, as shown in

Figure 43. No acid catalyzed reactions of toluene occurred. Given the fact that at these conditions no catalyst deactivation was detected, acid catalyzed reactions of toluene can be considered to cause catalyst deactivation. Despite the preferential physisorption of the aromatic

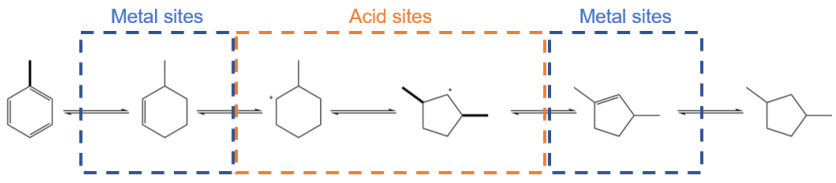

molecules onto the catalyst and complete toluene hydrogenation, the catalyst remained well balanced for *n*-octane conversion.

Figure 43: Possible predominant toluene reaction scheme under high hydrogen-to-hydrocarbon ratio.

Alternatively, with low hydrogen-to-hydrocarbon ratio, the catalyst was rapidly deactivated, likely due to preferential toluene adsorption on acid sites, and this effect was stronger at lower applied pressure. Toluene conversion was not complete under these conditions and the selectivity towards hydrogenation products was lower, however it remained relatively high. Hydrogenation products (Figure 42–A) were still the predominant product of toluene however, the reduced selectivity towards hydrogenation means that part of the converted toluene reacted directly on the acid sites of the catalyst (Figure 42-B) through transalkylation and disproportionation reactions yielding benzene and xylenes. These reactions significantly decrease the availability of acid active sites for the isomerization/cracking reactions of *n*-octane leading to the poisoning the catalyst and its fast deactivation, as observed with the time-on-stream tests shown in Figure 38. The results obtained are in line with what has been previously reported in literature (see section 2.4.3). It can be deduced that high excess of hydrogen will favor toluene hydrogenation, shifting the equilibrium of this reaction towards the products, and suppressing direct aromatic reaction on acid sites, which leads to deactivation.

Despite deactivation being observed across all operating conditions, the pressure impact was different at 270 °C and 290 °C. At lower temperature, pressure increase lead to a decrease in conversion meaning that the catalyst remained well-balanced. However, when temperature was 290 °C, a transition from ideal to non-ideal hydrocracking was noticed since higher pressure resulted in higher conversion. This shift in regime was confirmed by lower *n*-octane isomer selectivity.

The transition to non-ideal hydrocracking observed when hydrogen-to-hydrocarbon was 6.5 and at high temperature can be related to both the introduction of the aromatic component and the change in operating conditions. At the temperature of 270 °C, toluene hydrogenation lowers the amount of available metal sites which could induce a shift towards non-ideal hydrocracking however since toluene also reacts directly in active acid sides which decreases their availability, the overall ratio of available metal and acid sites is still high enough to ensure ideal hydrocracking. At the temperature of 290 °C, toluene continues to react on both metal and acid sites however, coupled with the effects of increasing temperature and pressure the ratio of concentrations of available metal and acid ratio is lowered to the point where non-ideal hydrocracking occurs.

Total pressure also had an observable impact on the deactivation of the catalyst: higher pressure led to less pronounced deactivation of the catalyst. The partial pressures of toluene and *n*-octane were kept constant across all experiments meaning that a change in total pressure only altered the partial pressure of inert gas (nitrogen). The deactivation of catalyst occurs as a result of coke formation which originates from the coke precursors produced via bimolecular reactions of toluene on catalyst acid sites. Higher amount of nitrogen, which is present at higher total

pressure, results in less frequent molecular collisions. This effect is assumed to be a reason for better stability of the catalyst at higher total pressure.

The addition of toluene showed that the main impact of this molecule occurred on the catalyst acid sites, which leads to deactivation and lower *n*-octane conversion. This effect can be minimized with high hydrogen excess since it promotes the hydrogenation reaction of toluene molecules, meaning that the used hydrogen-to-hydrocarbon ratio seems to be one of the main parameters for the control of aromatic admixture impact.

6. Conclusions and future work

The present work allowed for an insightful understanding of the effects of the addition of aromatic components on alkane hydrocracking by studying *n*-octane and toluene as model molecules.

The synthetized catalyst was characterized with different techniques which allowed for a better understanding of its physico-chemical properties. The addition of platinum did not affect the acidity of the catalyst. The catalyst elemental composition, zeolite surface area and porosity were in accordance with what was expected and with what had been previously reported. Despite having poor dispersion, the metal to acid sites ratio is higher than what has been proven to ensure ideal hydrocracking.

It was found that the addition of toluene to the alkane hydrocracking feed had no impact on the conversion of *n*-octane and on the occurrence of ideal hydrocracking when high hydrogen-to-hydrocarbon ratio was used. Time on stream tests proved that the catalyst stability was not affected by the introduction of the aromatic molecule in the feed. However, when the hydrogen partial pressure was reduced, by addition of nitrogen as diluent, rapid deactivation was observed across all the experimental conditions. The deactivation was more noticeable at lower applied pressure. It was also noticed a transition to non-ideal hydrocracking, at the temperature of 290 °C, as an increase in pressure lead to an increase in conversion.

It was found that toluene conversion is also dependent on hydrogen-to-hydrocarbon ratio. With high excess hydrogen, toluene conversion is complete and the selectivity towards hydrogenation products is 100%. When hydrogen-to-hydrocarbon ratio is lower, not all toluene is converted and small selectivity towards acid catalyzed products is detected. Despite hydrogenation products still being more prevalent on the reactor effluent, catalyst deactivation was observed. Toluene conversion and selectivity were highly dependent on the hydrogen-to-hydrocarbon ratio that was used. The findings of this experimental campaign showed that the toluene admixture impact can be reduced by increasing hydrogen-to-hydrocarbon ratio, promoting hydrogenation of aromatic molecule and avoiding catalyst deactivation.

Following this research and using the same catalyst, higher hydrogen-to-hydrocarbon ratios should be investigated, given that the one tested (H_2/HC = 6.5) led to rapid deactivation of the catalyst, so intermediate values of this parameter (between 6.5 and 200) should be used to

comprehend the optimal balance between hydrogen excess and good catalyst performance. Different feed mixture compositions could also be analyzed, such as a mixture of 3:2 n/n of *n*-alkane/aromatic, since aromatic components typically represent 40% of heavy oil composition [106], used as hydrocracking feed. However, given that this increases the concentration of aromatic component, the impacts on conversion, isomer selectivity and catalyst stability are expected to be more pronounced. It is worth noting that the conclusions presented in this thesis were obtained for a single catalyst which means that further investigation should be done to better understand the full impact of aromatic admixture on alkane hydrocracking.

7. References

[1] L. C. Castañeda, J. A. D. Muñoz, and J. Ancheyta, “Combined process schemes for upgrading of heavy petroleum” in *Fuel*, 2012, vol. 100, pp. 110–127. doi:10.1016/j.fuel.2012.02.022.

[2] M. Busto, J. M. Grau, J. H. Sepulveda, O. M. Tsendra, and C. R. Vera, “Hydrocracking of long paraffins over Pt-Pd/WO3-ZrO2 in the presence of sulfur and aromatic impurities” *Energy and Fuels*, vol. 27, no. 11, pp. 6962–6972, 2013, doi: 10.1021/ef401138v.

[3] I. Graa et al., “N-Heptane cracking over mixtures of HY and HZSM-5 zeolites: Influence of the presence of phenol” *Fuel*, vol. 94, pp. 571–577, 2012, doi: 10.1016/j.fuel.2011.11.033.

[4] C. G. Pernalete, J. Ibáñez, P. S. F. Mendes, K. M. van Geem, and J. W. Thybaut, “Hydrocracking of complex mixtures: From bulk properties, over fundamental kinetics to detailed product composition” *Catalysis Today*, vol. 378, pp. 189–201, 2021. doi: 10.1016/j.cattod.2021.06.010.

[5] US Energy Information Admnistration, “Hydrocracking is an important source of diesel and jet fuel” 2013. https://www.eia.gov/todayinenergy/detail.php?id=9650 (accessed Mar. 21, 2022).

[6] B. Pascal, M. Chaugny, L. Sancho, S. Roudier, “Best available techniques (BAT) reference document for the refining of mineral oil and gas industrial emissions: Industrial Emissions Directive 2010/75/EU (integrated pollution prevention and control)”. Publications Office, 2015.

[7] S. Bezergianni and A. Kalogianni, “Hydrocracking of used cooking oil for biofuels production” *Bioresour Technol*, vol. 100, no. 17, pp. 3927–3932, 2009. doi: 10.1016/j.biortech.2009.03.039.

[8] S. Bezergianni, S. Voutetakis, and A. Kalogianni, “Catalytic hydrocracking of fresh and used cooking oil” *Ind Eng Chem Res*, vol. 48, no. 18, pp. 8402–8406, 2009. doi: 10.1021/ie900445m.

[9] A. Galadima and O. Muraza, “Hydrocracking catalysts based on hierarchical zeolites: A recent progress” *Journal of Industrial and Engineering Chemistry*, vol. 61, pp. 265–280, 2018. doi: 10.1016/j.jiec.2017.12.024.

[10] G. W. Huber and A. Corma, “Synergies between bio- and oil refineries for the production of fuels from biomass” *Angewandte Chemie - International Edition*, vol. 46, no. 38. pp. 7184–7201, 2007. doi: 10.1002/anie.200604504.

[11] S. Bezergianni, A. Kalogianni, and I. A. Vasalos, “Hydrocracking of vacuum gas oil-vegetable oil mixtures for biofuels production” *Bioresour Technol*, vol. 100, no. 12, pp. 3036–3042, 2009. doi: 10.1016/j.biortech.2009.01.018.

[12] C. R. Chilakamarry, A. M. M. Sakinah, A. W. Zularisam, and A. Pandey, “Glycerol waste to value added products and its potential applications” *Systems Microbiology and Biomanufacturing*, vol. 1, no. 4. Springer, pp. 378–396, 2021. doi: 10.1007/s43393-021-00036-w.

[13] J. W. Thybaut et al., “Acid-metal balance of a hydrocracking catalyst: Ideal versus nonideal behavior” *Ind Eng Chem Res*, vol. 44, no. 14, pp. 5159–5169, 2005. doi: 10.1021/ie049375.

[14] J. Weitkamp, “Catalytic Hydrocracking-Mechanisms and Versatility of the Process” *Chem Cat Chem*, vol. 4, no. 3, pp. 292–306, 2012. doi: 10.1002/cctc.201100315.

[15] Corrosionpedia, “Hydrocracking” 2018. https://www.corrosionpedia.com/definition/1675/hydrocracking-petroleum-processing (accessed Mar. 24, 2022).

[16] L. Yan, Q. Zhang, W. Deng, Q. Zhang, and Y. Wang, “Catalytic valorization of biomass and bioplatforms to chemicals through deoxygenation” *Advances in Catalysis*, vol. 66, Academic Press Inc., 2020, pp. 1–108. doi: 10.1016/bs.acat.2020.09.002.

[17] R. Nickel, “Hydrogenolysis” 2019. https://chem.libretexts.org/Courses/Purdue/Purdue%3A_Chem_26605%3A_Organic_Chemistry_II_(Lipton)/Chapter_16._Oxidation_and_Reduction/16.6%3A_Hydrogenolysis (accessed Mar. 28, 2022).

[18] K. Atsonios, K. D. Panopoulos, A. Doukelis, and E. Kakaras, “Review of palladium membrane use in biorefinery operations” *Palladium Membrane Technology for Hydrogen Production, Carbon Capture and Other Applications: Principles, Energy Production and Other Applications*, Elsevier Ltd, 2015, pp. 345–368. doi: 10.1533/9781782422419.2.345.

[19] The essential Chemical Industry, “Cracking and related refinery processes” 2014. https://www.essentialchemicalindustry.org/processes/cracking-isomerisation-and-reforming.html (accessed Mar. 30, 2022).

[20] J. Clark, “Cracking Alkanes” 2020. https://www.essentialchemicalindustry.org/processes/cracking-isomerisation-and-reforming.html (accessed Mar. 30, 2022).

[21] The Editors of Encyclopedia Britannica, “Cracking Chemical Processes” 2020. https://www.britannica.com/technology/cracking-chemical-process (accessed Mar. 30, 2022).

[22] GlobalData, “Refinery Hydrocracking Units Capacity and Capital Expenditure Outlook with Details of All Operating and Planned Units” 2022. Available: https://www.globaldata.com/store/report/oil-and-gas-refinery-hydrocracking-units-market-analysis/ (sccessed: Mar. 30, 2022).

[23] GlobalData, “US leads globally with highest operational refinery FCCU capacity” 2021. https://www.offshore-technology.com/comment/us-leads-global-fccu-capacity/ (accessed Mar. 30, 2022).

[24] J. W. Thybaut and G. B. Marin, “Multiscale Aspects in Hydrocracking: From Reaction Mechanism Over Catalysts to Kinetics and Industrial Application” *Advances in Catalysis*, vol. 59, Academic Press Inc., 2016, pp. 109–238. doi: 10.1016/bs.acat.2016.10.001.

[25] A. de Lucas, P. Sánchez, F. Dorado, M. J. Ramos, and J. L. Valverde, “Effect of the metal loading in the hydroisomerization of n-octane over beta agglomerated zeolite based catalysts” *Applied Catalysis A: General*, vol. 294, no. 2, pp. 215–225, 2005. doi: 10.1016/j.apcata.2005.07.035.

[26] S. Sartipi, M. Makkee, F. Kapteijn, and J. Gascon, “Catalysis engineering of bifunctional solids for the one-step synthesis of liquid fuels from syngas: A review” *Catalysis Science and Technology*, vol. 4, no. 4. pp. 893–907, 2014. doi: 10.1039/c3cy01021j.

[27] H. González, J. Ramírez, A. Gutiérrez-Alejandre, P. Castillo, T. Cortez, and R. Zárate, “Selective hydroconversion of a model mixture and hydrotreated FCC gasoline for octane enhancement” *Catalysis Today*, 2004, vol. 98, no. 1-2 SPEC. ISS., pp. 181–191. doi: 10.1016/j.cattod.2004.07.032.

[28] E. Ocaranza, H. González, and J. Ramírez, “Hydroconversion of model mixtures of FCC gasoline over metal-zeolite catalysts. Reaction study and mathematical modelling” *Chemical Engineering Science*, 2004, vol. 59, no. 22–23, pp. 5679–5685. doi: 10.1016/j.ces.2004.07.048.

[29] E. N. Domoroshchina, V. V. Chernyshev, G. M. Kuzmicheva, A. V. Dorokhov, L. V. Pirutiko, G. V. Kravchenko and R. B Chumakov, “Changing the characteristics and properties of zeolite Y and nano-anatase in the formation of a nano-anatase/Y composite with improved photocatalytic and adsorption properties” *Applied Nanoscience*, vol. 8, pp. 19-31, 2018. doi: https://doi.org/10.1007/s13204-018-0648-5.

[30] E. Catizzone, S. Daele, M. Bianco, A. Michele, A. Aloise, M. Migliori, V. Valtchev and G. Giordano, “Catalytic application of ferrierite nanocrystals in vapour-phase dehydration of methanol to dimethyl ether,” *Applied Catalysis B*, vol. 243, pp. 273–282, 2019. doi: 10.1016/j.apcatb.2018.10.060.

[31] A. Primo and H. Garcia, “Zeolites as catalysts in oil refining,” *Chemical Society Reviews*, vol. 43, no. 22. Royal Society of Chemistry, pp. 7548–7561, 2014. doi: 10.1039/c3cs60394f.

[32] E. T. C. Vogt, G. T. Whiting, A. Dutta Chowdhury, and B. M. Weckhuysen, “Zeolites and zeotypes for oil and gas conversion” *Advances in Catalysis*, vol. 58, Academic Press Inc, 2015, pp. 143–314. doi: 10.1016/bs.acat.2015.10.001.

[33] H. Hattori and Y. Ono, “Catalysts and catalysis for acid-base reactions” *Metal Oxides in Heterogeneous Catalysis*, Elsevier, 2018, pp. 133–209. doi: 10.1016/B978-0-12-811631-9.00004-1.

[34] W. Julian Hatcher Jr and W. Julian Jr, “Hydrocracking of Normal Hexane and Cyclohexane Over Zeolite Hydrocracking of Normal Hexane and Cyclohexane Over Zeolite Catalysts. Catalysts” 1968. Available: https://digitalcommons.lsu.edu/gradschool_disstheses (accessed Mar. 30, 2022).

[35] Y. Lee et al., “Synthesis and catalytic behavior of ferrierite zeolite nanoneedles” *ACS Catal*, vol. 3, no. 4, pp. 617–621, 2013, doi: 10.1021/cs400025s.

[36] I. Georgieva, L. Benco, D. Tunega, N. Trendafilova, J. Hafner, and H. Lischka, “Multiple adsorption of NO on cobalt-exchanged chabazite, mordenite, and ferrierite zeolites: A periodic density functional theory study” *Journal of Chemical Physics*, vol. 131, no. 5, 2009. doi: 10.1063/1.3182850.

[37] H. Fjellvag, K. P. Lillerud, P. Norby, and K. Scrby, “Structural properties of some ferrierite-type zeolites” in *Zeolites*, vol. 9. Butterworth Publishers, pp 152-158,1989. doi: https://doi.org/10.1016/0144-2449(89)90066-3.

[38] A. Corma and A. Martinez, “Zeolites in refining and petrochemistry” *Studies in surface science and catalysis*, vol. 157. Elsevier, pp 337-366, 2005. doi:10.1016/S0167-2991(05)80018-7.

[39] V. Akhmedov and S. Al-Khowaiter, “Recent advances and future aspects in the selective isomerization of high n-alkanes” *Catalysis Reviews - Science and Engineering*, vol. 49, no. 1, pp. 33–139, 2007. doi: 10.1080/01614940601128427.

[40] A. de Lucas, J. L. Valverde, P. Sánchez, F. Dorado, and M. J. Ramos, “Hydroisomerization of n-octane over platinum catalysts with or without binder” *Applied Catalysis A: General*, vol. 282, no. 1–2, pp. 15–24, 2005. doi: 10.1016/j.apcata.2004.11.039.

[41] A. Lugstein, A. Jentys, and H. Vinek, “Hydroisomerization and cracking of n-octane and C 8 isomers on Ni-containing zeolites” *Applied Catalysis A: General*, vol. 176, pp. 119-128, 1998. doi: https://doi.org/10.1016/S0926-860X(98)00231-2.

[42] K.C. Park and S.K. Ihm, “Comparison of Pt/zeolite catalysts for n-hexadecane hydroisomerization,” *Applied Catalysis A: General*, vol.203, pp. 201-209, 2000. doi: https://doi.org/10.1016/S0926-860X(00)00490-7

[43] P. S. F. Mendes, J. M. Silva, M. F. Ribeiro, A. Daudin, and C. Bouchy, “Synergies, cooperation and other effects: a review for hydroconversion catalysts,” *Catalysis Today*, vol. 356. Elsevier B.V., pp. 260–270, 2020. doi: 10.1016/j.cattod.2019.08.055.

[44] J. H. Gary, G. E. Handwerk, and M. J. Kaiser, “Petroleum refining: technology and economics”, 2007, 5th edition, Taylor & Francis Group, Boca Raton, FL.

[45] G. C. Myers, W. E. Garwood, B. W. Rope, R. L. Wadlinger, and W. P. Hawthorne, “Stability of Hydrocracking Catalyst,” *Journal of Chemical Engineering Data*, vol. 7, no. 2, pp. 257-262, 1962. doi: https://doi.org/10.1021/je60013a030.

[46] T. Y. Yan, “The Promotional Effect of Water in Hydrocracking,” *Journal of Catalysis*, vol. 25, pp. 204-211, 1972. doi: https://doi.org/10.1016/0021-9517(72)90219-9.

[47] L. B. Galperin, “Hydroisomerization of n-decane in the presence of sulfur and nitrogen compounds,” *Applied Catalysis A: General*, vol. 209, pp. 257-268, 2001. doi: 10.1016/S0926-860X(00)00759-6.

[48] H. Coonradt and W. Garwood, “Mechanism of hydrocracking: Reactions of Paraffins and Olefins,” *Ind. Eng. Chem. Process Design and Development*, vol. 3, no.1, pp. 38-45, 1964. doi: https://doi.org/10.1021/i260009a010.

[49] F. Alvarez, F. R. Ribeiro, G. Perot, C. Thomazeau, and M. Guisnet, “Hydroisomerization and Hydrocracking of Alkanes: 7. Influence of the Balance between Acid and Hydrogenating Functions on the Transformation of n-Decane on PtHY Catalysts” *Journal of Catalysis*, vol. 162, no. 2, pp. 179-189, 1996. doi: https://doi.org/10.1006/jcat.1996.0275.

[50] R. A. Flinn, A. Larson, and H. Beuther, “The Mechanism of Catalytic Hydrocracking Catalytic hydrocracking,” *Industrial and Chemical Engineering*, vol. 52, no. 2, pp. 153-156, Feb. 1960. doi: https://doi.org/10.1021/ie50602a034.

[51] J. E. Denayer and G. Baron, “Adsorption of Normal and Branched Paraffins in Faujasite Zeolites NaY, HY, Pt/NaY and USY” *Adsorption*, vol.3, pp. 251-265, 1996. doi: https://doi.org/10.1007/BF01653628.

[52] I. Horiuti and M. Polanyi, “Exchange reactions of hydrogen on metallic catalysts” *Transactions of the Faraday Society*, vol. 30, pp. 1164–1172, 1934. doi: 10.1039/tf9343001164.

[53] B. Mattson et al., “Heterogeneous catalysis: The horiuti-polanyi mechanism and alkene hydrogenation,” *J Chem Educ*, vol. 90, no. 5, pp. 613–619, 2013. doi: 10.1021/ed300437k.

[54] J. J. H. B. Sattler, J. Ruiz-Martinez, E. Santillan-Jimenez, and B. M. Weckhuysen, “Catalytic dehydrogenation of light alkanes on metals and metal oxides,” *Chemical Reviews*, vol. 114, no. 20. American Chemical Society, pp. 10613–10653, 2014. doi: 10.1021/cr5002436.

[55] P. Weisz, “Polyfunctional Heteregenous Catalysis” *Advances in Catalysis*, vol.13, pp. 137-190, 1962. doi: https://doi.org/10.1016/S0360-0564(08)60287-4.

[56] J. F. Denayer, G. v. Baron, G. Vanbutsele, P. A. Jacobs, and J. A. Martens, “Evidence for Alkylcarbenium Ion Reaction Intermediates from Intrinsic Reaction Kinetics of C6-C9n-Alkane Hydroisomerization and Hydrocracking on Pt/H-Y and Pt/USY Zeolites,” *J Catal*, vol. 190, no. 2, pp. 469–473, 2000. doi: 10.1006/jcat.1999.2756.

[57] J. W. Thybaut, G. B. Marin, G. v. Baron, P. A. Jacobs, and J. A. Martens, “Alkene protonation enthalpy determination from fundamental kinetic modeling of alkane hydroconversion on Pt/H-(US)Y-zeolite,” *J Catal*, vol. 202, no. 2, pp. 324–339, 2001. doi: 10.1006/jcat.2001.3292.

[58] J. A. Martens and P. A. Jacobs, “2. Conceptual background for the conversion of hydrocarbons on heterogeneous acid catalysts”, *Theoretical Aspects of Heterogeneous Catalysis*, pp. 52-109, 1990, 1st edition, Van Nostrand Reinhold, New York, NY. doi: 10.1007/978-94-010-9882-3.

[59] J. Weitkamp, “Isomerization of Long-chain n-Alkanes on a Pt/CaY Zeolite Catalyst” *Ind Eng Chem Prod Des Dev*, vol. 21, no. 4, pp. 550-558, 1982. doi: https://doi.org/10.1021/i300008a008.

[60] D. M. Brouwer, “HF-SbF_5 Catalysed Isomerization n-butane-1-^{13}C” *Recueil des Travaux Chimiques des Pays-Bas*, vol. 87, no.12, pp. 1435-1444, 1968. doi: 10.1002/recl.19680871212.

[61] Y. v. Kissin, “Chemical Mechanisms of Catalytic Cracking over Solid Acidic Catalysts: Alkanes and Alkenes,” *Catal Rev Sci Eng*, vol. 43, no. 1–2, pp. 85–146, 2001. doi: 10.1081/CR-100104387.

[62] J. S. Buchanan, J. G. Santiesteban, and W. O. Haag, “Mechanistic Considerations in Acid-Catalyzed Cracking of Olefins” *Journal of Catalysis*, vol. 158, no. 1, pp. 279-287, 1996. doi: https://doi.org/10.1006/jcat.1996.0027.

[63] J. A. Martens, M. Tielen, and P. A. Jacobs, “Attempts to rationalize the distribution of hydrocracked products. III. Mechanistic aspects of isomerization and hydrocracking of branched alkanes on ideal bifunctional large-pore zeolite catalysts” *Catalysis Today*, vol. 1, no. 4, pp. 435-453, 1987. doi: https://doi.org/10.1016/0920-5861(87)80008-1.

[64] G. G. Martens, J. W. Thybaut, and G. B. Marin, “Single-event rate parameters for the hydrocracking of cycloalkanes on Pt/US-Y zeolites,” *Ind Eng Chem Res*, vol. 40, no. 8, pp. 1832–1844, 2001. doi: 10.1021/ie000799n.

[65] D. M. Brouwer and H. Hogeveen, “The Importance of Orbital Orientation as Rate Controlling Factor in Intramolecular Reactions of Carbonium Ions” *Recueil des Travaux Chimiques des Pays-Bas*, vol. 89, no. 2, pp. 211-224, 1970. doi: https://doi.org/10.1002/recl.19700890213.

[66] S. S. Arora and A. Bhan, “Kinetics of aromatics hydrogenation on HBEA,” *Journal of Catalysis*, vol. 383, pp. 24–32, 2020. doi: 10.1016/j.jcat.2019.12.039.

[67] P. Castaño, J. M. Arandes, B. Pawelec, M. Olazar, and J. Bilbao, “Kinetic modeling for assessing the product distribution in toluene hydrocracking on a Pt/HZSM-5 catalyst,” *Ind Eng Chem Res*, vol. 47, no. 4, pp. 1043–1045, 2008. doi: 10.1021/ie071154r.

[68] K. Toch, J. W. Thybaut, B. D. Vandegehuchte, C. S. L. Narasimhan, L. Domokos, and G. B. Marin, “A Single-Event Micro Kinetic model for ‘ethylbenzene dealkylation/xylene isomerization’ on Pt/H-ZSM-5 zeolite catalyst,” *Applied Catalysis A: General*, vol. 425–426, pp. 130–144, 2012. doi: 10.1016/j.apcata.2012.03.011.

[69] J. M. Silva Ribeiro, F. Ram, and R. E. Benazzi M Guisnet, “Transformation of an ethylbenzene-o-xylene mixture on HMOR and Pt-HMOR catalysts. Comparison with ZSM-5 catalysts” *Applied Catalysis A: General*, vol. 125, no. 1, pp. 15-27, 1995. doi: https://doi.org/10.1016/0926-860X(94)00259-2.

[70] G. G. Martens, G. B. Marin, J. A. Martens, P. A. Jacobs, and G. v. Baron, “A Fundamental Kinetic Model for Hydrocracking of C8 to C12 Alkanes on Pt/US-Y Zeolites,” *Journal of Catalysis*, vol. 195, no. 2, pp. 253–267, 2000. doi: 10.1006/jcat.2000.2993.

[71] T. F. Degnan and C. R. Kennedy, “Impact of catalyst acid/metal balance in hydroisomerization of normal paraffins,” AIChE Journal, vol. 39, no. 4, pp. 607–614, 1993. doi: 10.1002/aic.690390409.

[72] N. Korica, P. S. F. Mendes, J. de Clercq, and J. W. Thybaut, “Interplay of Metal-Acid Balance and Methylcyclohexane Admixture Effect on n-Octane Hydroconversion over Pt/HUSY,” *Ind Eng Chem Res*, vol. 60, no. 34, pp. 12505–12520, 2021. doi: 10.1021/acs.iecr.1c01775.

[73] J. Weitkamp, “The influence of chain length in hydrocracking and hydroisomerization of n-alkanes,” *Hydrocracking and Hydrotreating*, 1975, Washington, DC . doi: 10.1021/bk-1975-0020.ch001.

[74] J. F. Denayer, G. v Baron, W. Souverijns, J. A. Martens, and P. A. Jacobs, “Hydrocracking of n-Alkane Mixtures on Pt/H-Y Zeolite: Chain Length Dependence of the Adsorption and the Kinetic Constants,” *Ind Eng Chem Res*, vol. 36, no. 8, pp. 3242-3247, 1997. doi: https://doi.org/10.1021/ie960657m.

[75] P. Sánchez, F. Dorado, M. J. Ramos, R. Romero, V. Jiménez, and J. L. Valverde, “Hydroisomerization of C6-C8 n-alkanes, cyclohexane and benzene over palladium and platinum beta catalysts agglomerated with bentonite,” *Applied Catalysis A: General*, vol. 314, no. 2, pp. 248–255, 2006. doi: 10.1016/j.apcata.2006.08.025.

[76] A. Holló, J. Hancsók, and D. Kalló, “Kinetics of hydroisomerization of C 5-C 7 alkanes and their mixtures over platinum containing mordenite,” *Applied Catalysis A: General*, vol. 229, no. 1, pp. 93-102, 2002. doi: https://doi.org/10.1016/S0926-860X(02)00018-2.

[77] M. Guisnet and V. Fouche, “Isomerization of n-hexane on platinum dealuminated mordenite catalysts III. Influence of hydrocarbon impurities,” *Applied Catalysis*, vol. 71, no. 2, pp. 307-317, 1991. doi: https://doi.org/10.1016/0166-9834(91)85088-D.

[78] J. F. Denayer et al., “Adsorption Competition Effects in Hydroconversion of Alkane Mixtures on Zeolites,” *International Journal of Chemical Reaction Engineering*, vol. 1, no. article A36, 2003. doi: https://doi.org/10.2202/1542-6580.1061.

[79] J. F. Kriz, T. D. Pope, M. Stanciulescu, and J. Monnier, “Catalysts for the isomerization of C7 paraffins,” *Ind Eng Chem Res*, vol. 37, no. 12, pp. 4560–4569, 1998. doi: 10.1021/ie9803366.

[80] C. G. Walter, B. Coq, F. Figueras, and M. Boulet, “Competitive reaction of methylcyclohexane and n-hexane over alumina-supported platinum, iridium and ruthenium

catalysts," *Applied Catalysis A: General*, vol. 133, no. 1, pp. 95-102, 1995. doi: https://doi.org/10.1016/0926-860X(95)00180-8.

[81] C. Jiménez, F. J. Romero, R. Roldán, J. M. Marinas, and J. P. Gómez, "Hydroisomerization of a hydrocarbon feed containing n-hexane, n-heptane and cyclohexane on zeolite-supported platinum catalysts," *Applied Catalysis A: General*, vol. 249, no. 1, pp. 175–185, 2003. doi: 10.1016/S0926-860X(03)00177-7.

[82] N. Korica et al., "Mixture effects in alkane/cycloalkane hydroconversion over Pt/HUSY: Carbon number impact," *Fuel*, vol. 318, Jun. 2022, doi: 10.1016/j.fuel.2022.123651.

[83] R. H. Abudawood, "Hydroisomerization of alkanes over metal-loaded zeolite catalysts," 2010, PhD thesis, University of Manchester, Manchester.

[84] J.-K. Chen, A. M. Martin, and V. T. John', "A kinetic analysis of competitive reaction in intrazeolitic media," *Chemical Engineering Science*, vol. 45, no. 3, pp. 575-586, 1990. doi: https://doi.org/10.1016/0009-2509(90)87002-A.

[85] J. K. Chen, A. Martin, and V. John, "Modifications of n-Hexane Hydroisomerization over Pt/Mordenite as Induced by Aromatic Cofeeds" *Journal of Catalysts*, vol. 3, pp. 425–428, 1998. doi: https://doi.org/10.1016/0021-9517(88)90102-9.

[86] M. Busto, J. M. Grau, J. H. Sepulveda, O. M. Tsendra, and C. R. Vera, "Hydrocracking of long paraffins over Pt-Pd/WO3-ZrO2 in the presence of sulfur and aromatic impurities" *Energy and Fuels*, vol. 27, no. 11, pp. 6962–6972, 2013. doi: 10.1021/ef401138v.

[87] R. Galiasso Tailleur and J. R. Nascar, "The effect of aromatics on paraffin mild hydrocracking reactions (WNiPd/CeY-Al2O3)" *Fuel Processing Technology*, vol. 89, no. 8, pp. 808–818, 2008. doi: 10.1016/j.fuproc.2008.01.012.

[88] S. M. Waziri, A. M. Aitani, and S. Al-Khattaf, "Transformation of toluene and 1,2,4-trimethylbenzene over ZSM-5 and mordenite catalysts: A comprehensive kinetic model with reversibility" *Ind Eng Chem Res*, vol. 49, no. 14, pp. 6376–6387, 2010. doi: 10.1021/ie100527x.

[89] F. M. Almulla, V. I. Zholobenko, J. P. Waters, and A. A. Garforth, "Transalkylation of toluene with 1, 2, 4-trimethylbenzene over large pore zeolites with differing Si/Al ratios" *Chem Eng Trans*, vol. 57, pp. 943–948, 2017. doi: 10.3303/CET1757158.

[90] K. van der Borght, K. Toch, V. v. Galvita, J. W. Thybaut, and G. B. Marin, "Information-driven catalyst design based on high-throughput intrinsic kinetics" *Catalysts*, vol. 5, no. 4, pp. 1948–1968, 2015. doi: 10.3390/catal5041948.

[91] J. de Waele, T. Rajkhowa, and K. Toch, "High-Throughput Kinetic Setup (HTK-1): Manual and safety guidelines," 2015. Available: www.lct.ugent.be

[92] W. A. Dietz, "Response Factors for Gas Chromatographic Analyses" *Journal of Chromatographic Science*, vol. 5, no. 2, pp. 68-71, 1967. doi: https://doi.org/10.1093/chromsci/5.2.68.

[93] J. M. Lopes, "Introduction to Heterogeneous Catalysis", Advanced Chemical Engineering - Instituto Superior Técnico, Lisbon, 2021.

[94] J. Choma, J. Jagiello, and M. Jaroniec, "Assessing the contribution of micropores and mesopores from nitrogen adsorption on nanoporous carbons: Application to pore size analysis" *Carbon N Y*, vol. 183, pp. 150–157, 2021. doi: 10.1016/j.carbon.2021.07.020.

[95] P. Zhang, "Adsorption and Desorption Isotherms." 2016 [Online]. Available: http://www.keresearchgroup.com/uploads/4/8/4/5/48456521/160903_introduction_to_bet_isotherms.pdf. (accessed Jul. 09, 2022).

[96] M. J. Remy et al., “Dealuminated H-Y Zeolites: Relation between Physicochemical Properties and Catalytic Activity in Heptane and Decane Isomerization” *Journal of Physical Chemistry*, vol. 100, no. 20, pp. 12440-12447, 1996. doi: https://doi.org/10.1021/jp953006x.

[97] I. C. Neves, G. Botelho, A. v. Machado, and P. Rebelo, “Catalytic degradation of polyethylene: An evaluation of the effect of dealuminated Y zeolites using thermal analysis” *Mater Chem Phys*, vol. 104, no. 1, pp. 5–9, 2007. doi: 10.1016/j.matchemphys.2007.02.032.

[98] S. Morin, P. Ayrault, N. S. Gnep, and M. Guisnet, “Influence of the framework composition of commercial HFAU zeolites on their activity and selectivity in m-xylene transformation” *Applied Catalysis A: General*, vol. 166, no. 2, pp. 281-292, 1998. doi: https://doi.org/10.1016/S0926-860X(97)00263-9.

[99] N. Katada and M. Niwa, “Analysis of acidic properties of zeolitic and non-zeolitic solid acid catalysts using temperature-programmed desorption of ammonia” *Catalysis Surveys from Asia*, vol. 8, pp. 161-170, 2004. doi: https://doi.org/10.1023/B:CATS.0000038534.37849.16.

[100] W. Zhang and P. G. Smirniotis, “Effect of Zeolite Structure and Acidity on the Product Selectivity and Reaction Mechanism for n-Octane Hydroisomerization and Hydrocracking” *Journal of Catalysis*, vol. 182, no. 2, pp. 400-416, 1999. doi: https://doi.org/10.1006/jcat.1998.2337.

[101] The Editors of Encyclopaedia Britannica, “Crude oil - Britannica,” May 27, 2020. https://www.britannica.com/science/crude-oil/additional-info#history (accessed Jun. 18, 2022).

[102] L. Xu, Y. Li, J. Zhu, and Z. Liu, “Removal of Toluene by Adsorption/Desorption Using Ultra-stable Y Zeolite” *Transactions of Tianjin University*, vol. 25, no. 4, pp. 312–321, 2019. doi: 10.1007/s12209-019-00186-y.

[103] J. F. Denayer, W. Souverijns, P. A. Jacobs, J. A. Martens, and G. v Baron, “High-Temperature Low-Pressure Adsorption of Branched C 5-C 8 Alkanes on Zeolite Beta, ZSM-5, ZSM-22, Zeolite Y, and Mordenite” *Journal of Physical Chemistry*, vol. 102, no.23, pp. 4588-4597, 1998. doi: https://doi.org/10.1021/jp980674k.

[104] Engineering ToolBox, “Toluene - Thermodynamic properties” 2018. https://www.engineeringtoolbox.com/toluene-methylbenzene-properties-d_2095.html (accessed Jun. 23, 2022).

[105] V. Vesovic, “Octane” A-to-Z Guide to Thermodynamics, Heat and Mass Transfer, and Fluids Engineering, Begellhouse. doi: 10.1615/AtoZ.o.octane.

[106] R. G. Santos, W. Loh, A. C. Bannwart, and O. v. Trevisan, “An overview of heavy oil properties and its recovery and transportation methods” *Brazilian Journal of Chemical Engineering*, vol. 31, no. 3, pp. 571–590, 2014. doi: 10.1590/0104-6632.20140313s00001853.

Annex A – TEM Images

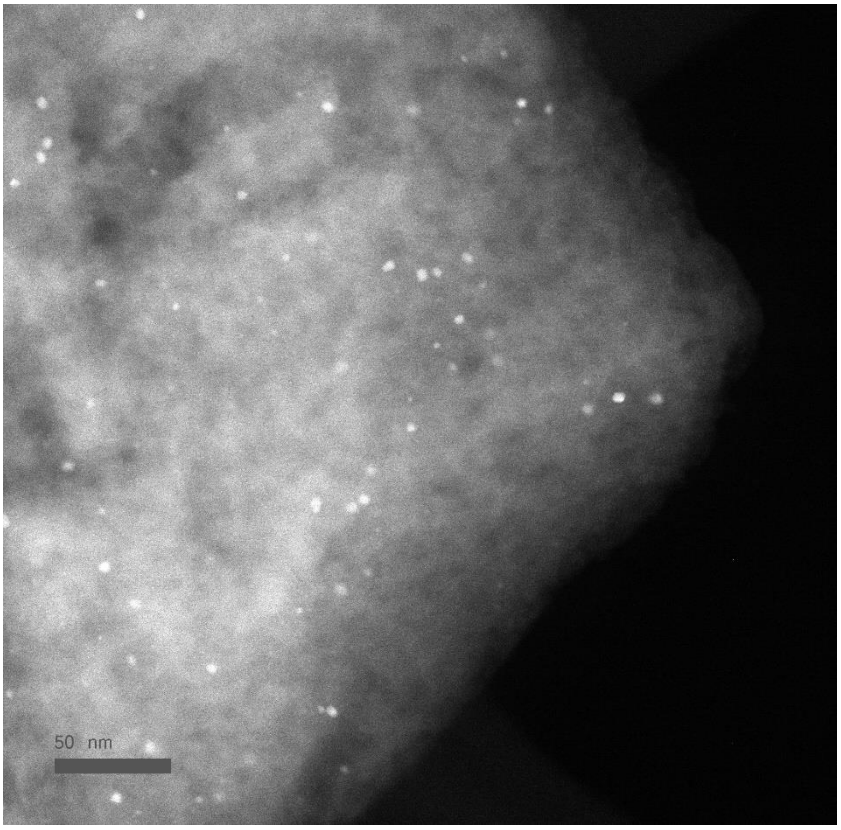

Figure A 1: TEM image of 0.3 wt% Pt/HUSY catalyst.

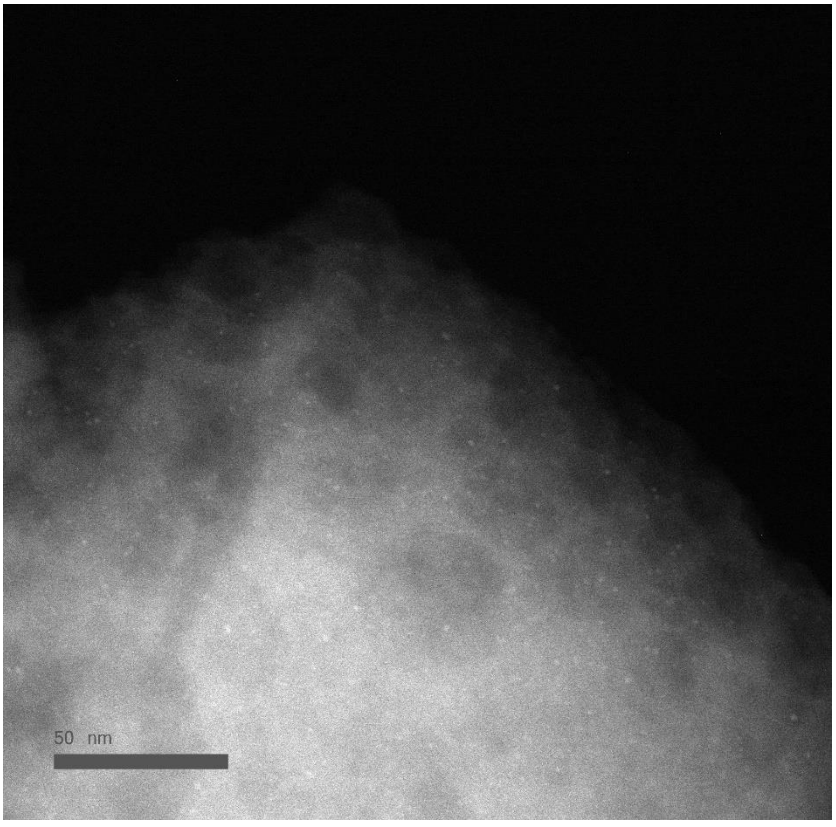

Figure A 2: TEM image of 0.3 wt% Pt/HUSY catalyst.

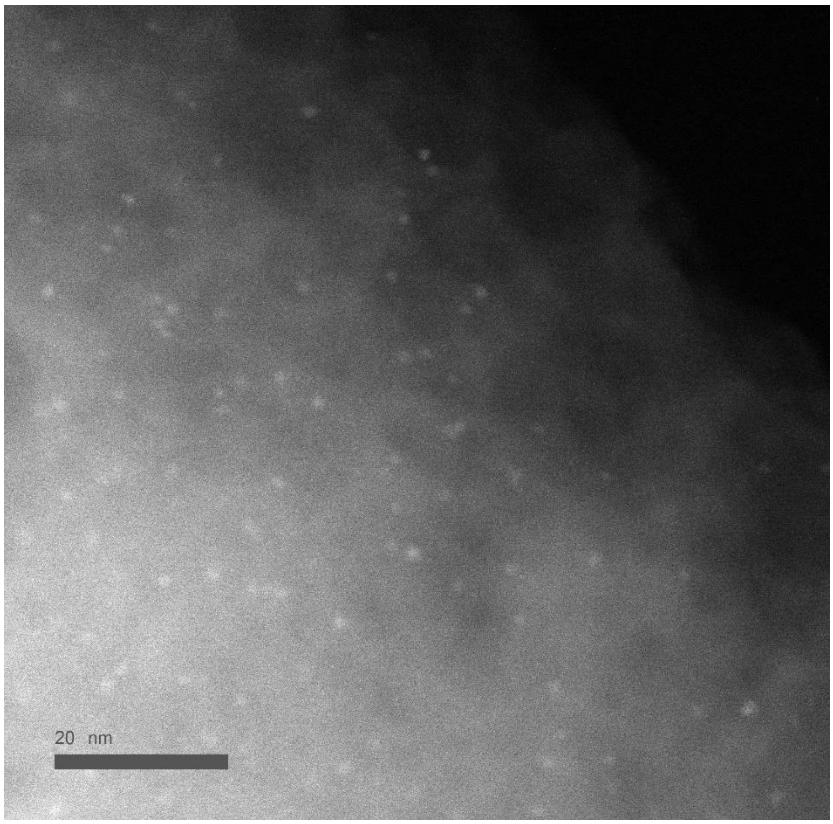

Figure A 3: TEM image of 0.3 wt% Pt/HUSY catalyst.